Possible application of stable isotope compositions for the identification of metal sources in soil

Liuwei Wang[a], Yuanliang Jin[a], Dominik J. Weiss[b,c], Nina J. Schleicher[b], Wolfgang Wilcke[d], Longhua Wu[e], Qingjun Guo[f,g], Jiubin Chen[h], David O'Connor[i], Deyi Hou[a*]

[a] *School of Environment, Tsinghua University, Beijing 100084, China*

[b] *Department of Earth Science & Engineering, Imperial College London, London SW7 2AZ, United Kingdom*

[c] *Civil and Environmental Engineering, Princeton University, New York*

[d] *Institute of Geography and Geoecology, Karlsruhe Institute of Technology (KIT), Reinhard-Baumeister-Platz 1, 76131 Karlsruhe, Germany*

[e] *Key Laboratory of Soil Environment and Pollution Remediation, Institute of Soil Science, Chinese Academy of Sciences, Nanjing 210008, China*

[f] *Center for Environmental Remediation, Institute of Geographic Sciences and Natural Resources Research, Chinese Academy of Sciences, Beijing 100101, China*

[g] *College of Resources and Environment, University of Chinese Academy of Sciences, Beijing 100049, China*

[h] *Institute of Surface-Earth System Science, School of Earth System Science, Tianjin University, Tianjin, 300072, China*

[i] *School of Real Estate and Land Management, Royal Agricultural University, Cirencester, GL7 1RS, United Kingdom*

** corresponding author (houdeyi@tsinghua.edu.cn)*

Phone: +86-010-62781159

Abstract

Metals in soil are potentially harmful to humans and ecosystems. Stable isotope measurement may provide “fingerprint” information on the sources of metals. In light of the rapid progress in this emerging field, we present a state-of-the-art overview of how useful stable isotopes are in soil metal source identification. Distinct isotope signals in different sources are the key prerequisites for source apportionment. In this context, Zn and Cd isotopes are particularly helpful for the identification of combustion-related industrial sources, since high-temperature evaporation-condensation would largely fractionate the isotopes of both elements. The mass-independent fractionation of Hg isotopes during photochemical reactions allows for the identification of atmospheric sources. However, compared with traditionally used Sr and Pb isotopes for source tracking whose variations are due to the radiogenic processes, the biogeochemical low-temperature fractionation of Cr, Cu, Zn, Cd, Hg and Tl isotopes renders much uncertainty, since large intra-source variations may overlap the distinct signatures of inter-source variations (i.e., blur the source signals). Stable isotope signatures of non-metallic elements can also aid in source identification in an indirect way. In fact, the soils are often contaminated with different elements. In this case, a combination of stable isotope analysis with mineralogical or statistical approaches would provide more accurate results. Furthermore, isotope-based source identification will also be helpful for comprehending the temporal changes of metal accumulation in soil systems.

Keywords: stable isotopes; source apportionment; heavy metals; isotope fractionation; soil contamination.

1 Introduction

Soil contamination is a public health concern and threat to sustainable development. In order to ensure healthy lives and promote well-being, the United Nations has set an ambitious goal to reduce the number of illnesses and deaths from soil contamination over the next decade (UN 2015). Potentially toxic elements in soil, including metals and metalloids, have aroused much attention owing to their toxicity and environmental persistence (Jing et al. 2019; Liu et al. 2019b; Wang et al. 2020b; Wang et al. 2019d; Zhang et al. 2020b). Moreover, they can bioaccumulate along food chains, thus aggravating the risk they present. Toxic metals such as cadmium (Cd), mercury (Hg) and lead (Pb) are among the World Health Organization's ten chemicals of major public health concern, because of the negative effects on neurologic, renal, skeletal and respiratory systems (O'Connor et al. 2020; WHO 2017). It is imperative to manage the risks associated with toxic metals wisely. To achieve this goal, it is valuable to understand the sources of metals in soil.

Metals in soil can originate from various sources, either natural or anthropogenic (Hou et al. 2020a; Jia et al. 2020b). Rock weathering is the most important natural origin of toxic elements, with the lithology of the parent rock affecting the type of metal, the susceptibility to weathering, and the geochemical properties of the soil (Alloway 2013; Jia et al. 2020b). Human activities, such as coal combustion (Vanek et al. 2016), nonferrous metal mining and smelting (Liu et al. 2013), vehicle traffic (De Silva et al. 2016), e-waste processing (Zhou et al. 2021), land irrigation with contaminated water

(Malan et al. 2015) and application of impure mineral fertilizers (Atafar et al. 2010), are exogenous inputs that increase the trace metal load of soils. These can be either point or non-point sources of pollution (Sherameti and Varma 2015; Zhang et al. 2019a).

Isotope ratio analysis (IRA) is a powerful tool to investigate the “fingerprints” of metals in environmental samples (Chen et al. 2018; Hoefs 2018; Weiss et al. 2008). Numerous efforts have been made to distinguish the sources of metals in soil, water and air on the basis of isotopic variations among various environmental samples. The most widely used approach is the analysis of the Pb isotope mixture, because the markedly different isotope signals of different materials, which are attributable to the fact that three of four Pb isotopes originate from radioactive decay chains, were early analytically accessible (Cheng and Hu 2010; Schoene 2014). Moreover, in-situ fractionation of Pb isotope ratios in soils can usually be neglected, because the radiogenic differences in Pb isotope composition are big relative to the small isotope fractionation induced by biogeochemical processes (Cheema et al. 2020; Wiederhold 2015). Provided that the Pb contamination of soil can be attributed to a two- or three-end-member mixture of different sources, the individual Pb sources can be quantified (Cheng and Hu 2010; Stückrad et al. 2010; Wilcke et al. 2001). With the development of advanced mass spectrometers with high precision (i.e., multi-collector inductively coupled plasma-mass spectrometry (MC-ICP-MS)), other stable metal isotopes, such as Zn, Cd, Tl and Hg, have also emerged as tracers for anthropogenic contamination (Li et al. 2019; Mihaljevic et al. 2019; Wiggenhauser et al. 2019).

This review summarizes the current state-of-the-art of the use of stable isotopes for soil metal source identification purposes, with a focus on non-radiogenic metal isotopes. The phenomenon of isotope variation (either induced by fractionation or radiogenic processes) and implications for source apportionment are explored in-depth. The simultaneous source identification of multi-elements, and the posterior disentanglement of temporally changing metal sources are addressed. Finally, several challenges and potential research directions, including the better selection of a suitable isotope for source identification, and the joint application of multi-isotopes are put forward.

2 Basic concepts and analysis methods

2.1 Background

Isotopes of an element are defined as atoms with the same number of protons but a different number of neutrons (Hoefs 2018). Isotopes can be divided into two categories. Stable isotopes had been created by the by the big bang and remain “stable” since then, while radioactive isotopes continuously decay into daughter isotopes of other elements (White 2015). Most elements in the periodic table consist of more than one stable isotope, but some elements occur monoisotopically (e.g., Be, F, Na, Al, P, Sc, Mn, Co, As, Y, Nb, Rh, I, Cs, Pr, Tb, Ho, Tm, Au, Bi, Pa).

Geochemical processes have led to subtle variations in isotope ratios among different environmental samples (Hoefs 2018; White 2015). With the rapid development of advanced isotopic detection tools (Section 2.2), these subtle variations became

112 analytically accessible for soil scientists. By convention, the small variations in stable
113 isotope ratios of non-radiogenic metals are expressed as delta values (Eq. 1):

114 $$\delta^{x}E = \left(\frac{R_{sa}^{x/y}}{R_{st}^{x/y}} - 1\right) \times 1000 \quad (1)$$

115 Where E refers to the element; x, y refers to the mass number (proton & neutron) of
116 the two isotopes of the element, respectively; R refers to the abundance ratio between
117 isotope x and isotope y; sa refers to the sample, and st refers to the arbitrarily selected
118 and internationally agreed standard reference material.
119 The convention was introduced early in the research of non-radiogenic isotopes of
120 non-metal stable isotopes such as H and O by Craig (1961) to magnify the small
121 differences in isotope ratios. The standard reference materials are often provided by
122 agencies such as the Institute for Reference Materials and Measurements (IRMM),
123 European Reference Materials (ERM) (in Europe) and the National Institute of
124 Standards and Technology (NIST) (in USA) (Meier-Augenstein and Schimmelmann
125 2019; Vogl and Pritzkow 2010).
126 For most metals, variations in isotope ratios among environmental samples are caused
127 by fractionation processes, such as evaporation/condensation,
128 dissolution/precipitation, redox processes, adsorption/desorption, and biological
129 cycling (except for Sr and Pb, where radiogenic processes play a vital role)
130 (Wiederhold 2015). Isotope fractionation is the partitioning of isotopes between two
131 chemical species or physical phases (e.g., free Cd^{2+} vs organo-Cd complexes, Cu^{+} vs
132 Cu^{2+}, or liquid vs vapor during evaporation/condensation processes, referred to as A

and B), which is caused either by the separation of isotopes in equilibrium systems (equilibrium fractionation) or during incomplete chemical or physical processes such as diffusion in soil solution or biological metabolism (kinetic fractionation) (Cheema et al. 2020; Hoefs 2018; Wiederhold 2015). Equilibrium fractionation is caused by isotope exchange reactions favoring the heavy isotopes in stable bonding environments, while kinetic fractionation is induced by the different reaction rates of isotopes favoring the light isotopes in the product.

Both equilibrium and kinetic fractionation are driven by the mass of isotopes (mass-dependent fractionation (MDF)). The apparent isotope fractionation by an equilibrium or kinetic process is frequently given as shown in Eq. (2).

$$\Delta^{x/y}E_{A-B} = \delta^{x/y}E_A - \delta^{x/y}E_B \quad (2)$$

For some metal isotopes (e.g. Hg, U, Tl), fractionation can also be mass-independent. The mechanisms involved in mass-independent fractionation (MIF) are not fully understood, but the nuclear volume effect (NVE) as well as the magnetic isotope effect (MIE) may contribute to this phenomenon. Nuclear volume expands with the increased number of neutrons, but the expansion caused by odd isotopes would be smaller than that for an even isotope, thus resulting in NVE-induced MIF. In contrast, MIE would fractionate isotopes due to their nuclear spin and magnetic moment (Hoefs 2018). For a mechanistic understanding of NVE and MIE, we refer readers to Bigeleisen (1996) and Buchachenko (2001), who have provided in-depth discussions.

2.2 Isotope analysis methods

The development of metal isotope geochemistry partly relies on analytical improvements in mass spectroscopy (MS). Among the plethora of MS techniques developed in the 20th century, thermal ionization mass spectroscopy (TIMS) was once regarded as the only reliable way for the precise determination of isotope ratios of metals. The purified sample solution is loaded onto the metal filament, which will be heated as the ionization source to the mass spectrometer (Figure S1). Since the late 1990s, multi-collector inductively coupled plasma mass spectrometer (MC-ICP-MS) has become available as an alternative to TIMS for metal isotope analysis (Hirata 1996; Walder et al. 1993), and has emerged as the most widely adopted technique in stable isotope studies in the 21st century (Irrgeher and Prohaska 2016; Yang 2009). Samples are introduced directly in solutions and ionized by an argon plasma. Compared with quadrupole-based ICP-MS (ICP-QMS) with single collector, both TIMS and MC-ICP-MS adopt a multi-collector setup, enabling the simultaneous quantification of different isotopic masses (the key to achieving the required high precision of ~0.1‰) (Figure S1) (Wiederhold 2015; Yang et al. 2018).

High-quality pretreatment is the prerequisite for the determination of metal stable isotopes. For soil samples, digestion (e.g., using mixtures of strong acids including hydrofluoric acid, HF) or extraction techniques (e.g., sequential extraction, acid leaching) would bring metals to solutions. After that, the liquid samples usually must be further purified using element-specific ion exchange chromatography (Figure S2)

(Li et al. 2019) to separate the target from other elements, which potential interfere in the measurement of the target element. Once the sample solution with various interfering cations passes through the ion exchange resin (e.g., AG MP-1 anion exchange resin) (Bio-Rad Laboratories 2020), the ions will partition between the liquid (i.e., solution) and solid (i.e., resin) phase. Due to the element-specific partitioning coefficients, different elements will be separated during the elution process (Figure S2) (Li et al. 2019). The key to the success of this process is a high recovery (usually >95%) of the target element to avoid any artificial isotope fractionation and low procedural blank values. To reach the latter, the digestion and sample purification are done in metal-free clean-air environment. In the later measurement with MC-ICP-MS the instrumental drift and the mass-specific measurement bias must be corrected with the help of sample bracketing and isotope doping/spiking approaches, in which non-target isotopes of the same element or of another element with similar mass are added to the sample prior to measurement. For detailed discussion regarding sample pretreatment, isotope analysis instrumentation and mass bias correction methods, we refer readers to Irrgeher and Prohaska (2016) and Yang et al. (2018).

2.3 Source apportionment strategies

Source apportionment is based on variations in isotope ratios amongst environmental samples. If the individual source signals are sufficiently distinct, source contributions can be calculated with mixing models. In the simplest scenario, if the isotope ratios of two sources (e.g., natural *vs* anthropogenic) are known, the contribution of each source

to soil metal contamination can be calculated using a simple binary mixing model (Eq. 3-4) (Weiss et al. 2008; Wiederhold 2015):

$$\delta_{soil} = \delta_A \times f_A + \delta_B \times f_B \quad (3)$$

$$f_A + f_B = 1 \quad (4)$$

where δ_{soil} refers to the δ value in soil, δ_A, δ_B represents the δ values of the sources A and B, f_A and f_B are contribution rate of sources A and B to soil metal accumulation, respectively. Given the measured values of δ_{soil}, δ_A and δ_B, the contribution rates can be calculated quantitatively (Eq. 5-6):

$$f_A = \frac{\delta_{soil} - \delta_B}{\delta_A - \delta_B} \quad (5)$$

$$f_B = \frac{\delta_{soil} - \delta_A}{\delta_B - \delta_A} \quad (6)$$

However, this simple two-end model cannot provide information on exact contributions of multiple anthropogenic sources (e.g., coal combustion, traffic activities, mining and smelting, irrigation, fertilization, etc.). The prerequisite of a binary model can be tested by plotting the reverse of the target element concentration *vs* the isotope ratio of this element. If there is a close linear correlation, it can be assumed that there are indeed only two sources. If not, there are either more sources or other processes that blur the source signals. In this context, much more complicated source apportionment models have been proposed:

1) Mass balance-based tertiary mixing model (Li et al. 2011):

Assuming W_{soil} kilograms of contaminated soil sample with metal concentration c_{soil} is a mixture of W_N kilograms of natural soil with metal concentration c_N, W_A

kilograms of dust from anthropogenic source A with metal concentration c_A, W_B kilograms of dust from anthropogenic source B with metal concentration c_B, soil mass balance (Eq. 7), metal mass balance (Eq. 8) and aforementioned mixing law of isotope ratio (Eq. 9) enable the quantitative calculation of three sources:

$$W_{soil} = W_N + W_A + W_B \quad (7)$$

$$W_{soil} \times c_{soil} = W_N \times c_N + W_A \times c_A + W_B \times c_B \quad (8)$$

$$\delta_{soil} = \frac{W_N \times c_N}{W_{soil} \times c_{soil}} \times \delta_N + \frac{W_A \times c_A}{W_{soil} \times c_{soil}} \times \delta_A + \frac{W_B \times c_B}{W_{soil} \times c_{soil}} \times \delta_B \quad (9)$$

Eq. 7-9 can also be expressed using contribution rates f_N, f_A and f_B (Eq. 10-12):

$$\frac{f_N \times c_{soil}}{c_N} + \frac{f_A \times c_{soil}}{c_A} + \frac{f_B \times c_{soil}}{c_B} = 1 \quad (10)$$

$$f_N + f_A + f_B = 1 \quad (11)$$

$$\delta_N \times f_N + \delta_A \times f_A + \delta_B \times f_B = \delta_{soil} \quad (12)$$

This system with three independent equations and three unknowns (i.e., f_N, f_A, f_B) will have a unique solution.

2) Tertiary mixing model (with multi-isotopes) (Luo et al. 2015; Wang et al. 2019a):

Another feasible way to have a unique solution to each source contribution is to add the number of independent equations through measuring multi-isotopes (Eq. 13-15):

$$\delta_{1N} \times f_N + \delta_{1A} \times f_A + \delta_{1B} \times f_B = \delta_{1soil} \quad (13)$$

$$\delta_{2N} \times f_N + \delta_{2A} \times f_A + \delta_{2B} \times f_B = \delta_{2soil} \quad (14)$$

$$f_N + f_A + f_B = 1 \quad (15)$$

where δ_1, δ_2 refer to different isotopes.

3) Isosource model (Chen et al. 2018; US EPA 2017):

Isosource aims to calculate the contributions of each sources in an underdetermined system (there are fewer independent equations than unknowns). As an open-access source apportionment software recommended by US EPA, it reports all the possible combinations of each source contributions within a small "mass balance tolerance". The basic equations in the software are as follows (Eq. 16-17):

$$\delta_{soil} = \delta_1 \times f_1 + \delta_2 \times f_2 + \cdots + \delta_n \times f_n \quad (16)$$

$$f_1 + f_2 + \cdots + f_n = 1 \quad (17)$$

For more information regarding this model, we refer readers to (US EPA 2016) and (US EPA 2017).

3 Stable isotope analysis for soil metal source apportionment

3.1 Chromium (atomic number Z = 24)

Chromium has four stable isotopes, including ^{50}Cr (4.3%), ^{52}Cr (83.8%), ^{53}Cr (9.5%) and ^{54}Cr (2.4%) (Hoefs 2018). Chromium isotope variations are described as follows (Eq. 18):

$$\delta^{53}Cr = \left(\frac{(^{53}Cr/^{52}Cr)_{sample}}{(^{53}Cr/^{52}Cr)_{standard}} - 1 \right) \times 1000 \quad (18)$$

The internationally used reference material for Cr is the NIST SRM 979 standard (Hoefs 2018; Qin and Wang 2017). Chromium is a redox-sensitive element, existing in the environment as Cr(III) and Cr(VI). Hexavalent oxyanions (i.e., CrO_4^-, $HCrO_4^{2-}$) are highly mobile and toxic, while the trivalent Cr^{3+} is the dominant form in minerals with low mobility (Alloway 2012). Redox transformation is the major fractionation mechanism for this element (Qin and Wang 2017).

According to the literature reviewed, Cr isotopes are rarely used for soil metal source identification purposes as described in Section 2.3. This is probably because the fractionation during redox transformation of this element would be significant, fading the distinct isotope signatures among different sources. For instance, the Cr isotope signature of groundwater in the vicinity of a coal-fired power plant ($\delta^{53}Cr_{NIST\ 979} = 1.80$) was heavier than both natural spring ($\delta^{53}Cr_{NIST\ 979} = 1.15$) and anthropogenic source of fly ash ($\delta^{53}Cr_{NIST\ 979} = 0.55$) as a result of Cr(VI) reduction, making it impossible for source apportionment (Kazakis et al. 2017).

In comparison, Cr isotope analysis has been extensively used for the process tracing of redox transformation between Cr(III) and Cr(VI) species. During Cr(VI) reduction processes, the oxyanion CrO_4^{2-} with lighter ^{52}Cr would be reduced more quickly than the oxyanion with heavier ^{53}Cr. Therefore, the products Cr(III) would be isotopically lighter (Ellis et al. 2002; Jonhson and Bullen 2004). Hence many successful attempts have been made to monitor Cr(VI) reduction (especially in groundwater) with Cr isotope compositions (Berna et al. 2010; Čadková and Chrastný 2015; Heikoop et al. 2014; Jamieson-Hanes et al. 2012; Raddatz et al. 2011). For further information regarding Cr isotope-based process tracing, we refer readers to Wiederhold (2015) and Qin and Wang (2017).

3.2 Copper (Z = 29)

There are two stable isotopes of copper (Cu), namely ^{63}Cu (69.1%) and ^{65}Cu (30.9%) (Hoefs 2018). Variations in Cu isotope are typically depicted as follows (Eq. 19):

$$\delta^{65}Cu = \left(\frac{(^{65}Cu/^{63}Cu)_{sample}}{(^{65}Cu/^{63}Cu)_{standard}} - 1 \right) \times 1000 \quad (19)$$

Usually, Cu isotope ratio are given relative to NIST SRM 976 Cu solution, which is, however, no longer available. ERM AE 633 and ERM AE 647 are also used, which have been calibrated against NIST SRM 976 (Hoefs 2018; Moeller et al. 2012).

Low-temperature fractionation is the major cause of Cu isotopic variations. Adsorption onto soil minerals and organic matter (Bigalke et al. 2010; Li et al. 2015), transformation of Cu(I) and Cu(II) species (Kusonwiriyawong et al. 2016; Zhao et al. 2019b), mineral dissolution (Viers et al. 2018; Wall et al. 2011) and biological activities (Jouvin et al. 2012; Navarrete et al. 2011) can lead to large fractionation (Figure 1, all isotope ratios are converted to $\delta^{65}Cu_{NIST\,976}$). The $\delta^{65}Cu_{NIST\,976}$ values of most samples vary from -2‰ to +2‰ (Figure 1). In rock and ore samples, a much larger variation in $\delta^{65}Cu_{NIST\,976}$ values has been reported (from -6.4‰ to +19.4‰) (Figure 1). Considering that the variations caused by low-temperature fractionation within a single source are usually much larger than the inter-source variations (i.e., the isotopic variations between different sources), source identification using Cu isotopes may be difficult. A limited number of studies have attempted to identify Cu sources using isotope analysis but have failed. For instance, Dótor-Almazán et al. (2017) found that the $\delta^{65}Cu_{NIST\,976}$ values of mine tailings fell within a wide range of -1.19‰ ~ +0.91‰. The intra-source fractionation of Cu isotopes during the diverse low-temperature processes used in mining caused such large variations. It was impossible for source apportionment to be undertaken since this range overlapped with isotopic signatures

of natural sources (-0.09‰ ~ +0.54‰ for parent rocks). Overall small variations of the $\delta^{65}Cu$ values and comparatively large intra-source variations lead to overlapped Cu isotope ratios between natural (e.g., bedrock) and various anthropogenic sources, rendering source tracking difficult or impossible.

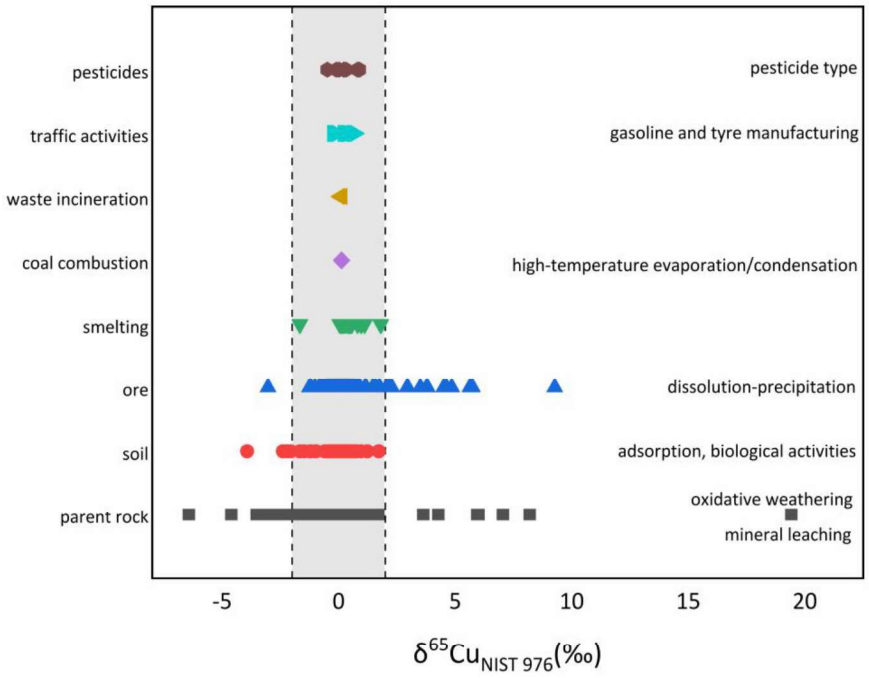

Figure 1 Variations in Cu isotopic signatures among environmental samples. All isotope ratios are converted to $\delta^{65}Cu_{NIST\,976}$. Compared with high-temperature mass-dependent isotope fractionation, low-temperature processes, such as mineral dissolution & precipitation, oxidation & reduction, and adsorption are the major causes of Cu isotope fractionation. The $\delta^{65}Cu_{NIST\,976}$ value of most samples fell within -2‰ ~ +2‰, except for some rock and ore samples. Data sources: parent rock (Bigalke et al. 2010; Dótor-Almazán et al. 2017; Liu et al. 2014; Lv et al. 2016; Mathur et al. 2012;

312 Šillerová et al. 2017); soil (Bigalke et al. 2013; Bigalke et al. 2010; Bigalke et al. 2011;
313 Blotevogel et al. 2018; Dótor-Almazán et al. 2017; Fekiacova et al. 2015; Kribek et al.
314 2018; Petit et al. 2013; Šillerová et al. 2017; Vance et al. 2016); ore (Dótor-Almazán et
315 al. 2017; Maréchal et al. 1999; Mason et al. 2005; Wilson et al. 2016; Zhu et al. 2000);
316 smelting (Bigalke et al. 2010; Fekiacova et al. 2015; Kribek et al. 2018; Zeng and Han
317 2020); coal combustion (Fekiacova et al. 2015; Šillerová et al. 2017); waste
318 incineration (Fekiacova et al. 2015); traffic activities (Dong et al. 2017); pesticides
319 (Blotevogel et al. 2018).
320
321 **3.3 Zinc (Z = 30)**
322 Zinc has five stable isotopes, namely ^{64}Zn (48.6%), ^{66}Zn (27.9%), ^{67}Zn (4.1%), ^{68}Zn
323 (18.8%), ^{70}Zn (0.6%) (Hoefs 2018). Zn isotope variations are usually depicted as the
324 $\delta^{66}Zn$ value (Eq. 20):
325 $$\delta^{66}Zn = \left(\frac{(^{66}Zn/^{64}Zn)_{sample}}{(^{66}Zn/^{64}Zn)_{standard}} - 1\right) \times 1000 \quad (20)$$
326 The JMC-Lyon and the IRMM-3702 standard are used as international standard
327 materials for Zn isotopes (Araújo et al. 2019; Hoefs 2018).
328 Evaporation/condensation during coal combustion and Zn smelting result in strong Zn
329 isotope fractionation of stack emissions, which is useful for the source apportionment
330 of coal combustion and smelting-induced soil contamination (Figure 2, all isotope ratios
331 are converted to $\delta^{66}Zn_{JMC-Lyon}$). During coal combustion, organic matter-bound
332 heavier Zn isotopes tend to be preferentially released to the gaseous phase, resulting

in higher $\delta^{66}Zn$ values in fly ash as compared to the original coal (Borrok et al. 2010; Gonzalez and Weiss 2015) (Figure 2). The flue gas samples from a Pb-Zn refinery were enriched in lighter Zn isotopes compared with the original ore samples, since lighter isotopes are more likely to be released during high-temperature (1300 K) volatilization/condensation in the smelter (Mattielli et al. 2009). Other geochemical processes, such as dissolution, pH-dependent hydration, adsorption and biological activities also contribute to the fractionation (Bigalke et al. 2010; Desaulty and Petelet-Giraud 2020; Hoefs 2018; Imseng et al. 2019b; Li et al. 2019). For instance, primary sphalerite dissolution and reprecipitation lead to large variations in $\delta^{66}Zn$ values for secondary Zn-containing minerals (Mondillo et al. 2018) (Figure 2). Heavier Zn isotopes are more likely to be adsorbed onto oxides, clay, carbonates and silicates due to the preferential incorporation of heavier Zn into the fourfold-coordinated tetrahedral complexes (Bryan et al. 2015; Gou et al. 2018). Microorganisms and plants may passively uptake lighter isotopes of Zn when diffusive transport dominates. In comparison, if Zn concentrations are relatively low, organisms may actively uptake heavier ones with the help of membrane transport proteins (Jouvin et al. 2012; Tang et al. 2016). Furthermore, heavier Zn isotopes are more likely to form complexes with the phytosiderophore that can be easily uptaken by rice plants (Marković et al. 2017). For detailed discussions on Zn isotope fractionation mechanisms, we refer readers to Desaulty and Petelet-Giraud (2020).

Zn isotope ratios have been shown to be more effective in soil metal source

identification than Cu isotope ratios, especially when industrial sources (e.g., coal combustion, smelting, incineration) play a dominant role in soil contamination (Figure 2). For instance, Araújo et al. (2018) found that the $\delta^{66}Zn_{JMC-Lyon}$ values of the contaminated mangrove sediments (+0.36‰ ~ +0.84‰) fell between those of natural detrital source (+0.28‰) and anthropogenic electroplating activities (+0.86‰), making it possible for source apportionment with a simple mixing model. Similarly, Bigalke et al. (2010) were able to explain the $\delta^{66}Zn$ values of the Oa horizon (the most decomposed organic horizon in forests), the mineral soil and the bedrock in Slovakia as a mixture of the two end members (i.e., Zn-isotopically light emissions of a brass foundry and Zn-isotopically heavy bedrock). However, Bigalke et al. (2010) also cautioned that the smelter signature was overprinted by in-situ biogeochemical Zn fractionation in the Oi and Oe horizons (little to intermediately decomposed organic horizons). Xia et al. (2020) observed that the distinct $\delta^{66}Zn_{IRMM-3702}$ values among tailings (-0.42‰), dust (-0.24‰) and the reference clean soil (-0.16‰) samples enabled the quantitative estimation of mining-induced contamination in the vicinity of a Zn mine. However, compared with industrial sources with unique Zn isotope ratios, Zn isotopic compositions of other sources (e.g., waste incineration, traffic activities, fertilizers) may not be “distinct enough” for source identification (Figure 2).

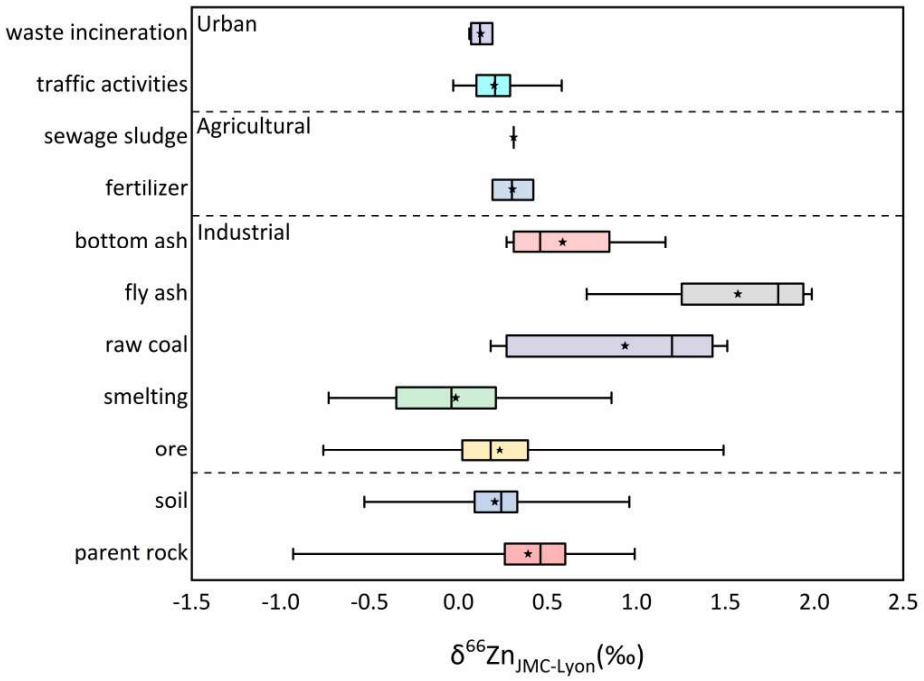

372

373 Figure 2 Stable Zn isotope ratios of various samples. All isotope ratios are converted
374 to $\delta^{66}Zn_{JMC-Lyon}$. Minimum, first quartile, median, third quartile and the maximum
375 values are presented as vertical bars, while the mean values are shown as the stars
376 within the box. Compared with industrial emissions (i.e., coal combustion, mining and
377 metal smelting), Zn isotopic signatures of other sources may not be distinct enough.
378 Relatively large variations in ore samples may result from the dissolution and
379 precipitation of sulfide minerals. Fly ash samples tend to be isotopically heavier, while
380 bottom ash samples are lighter than the raw coal, which is probably because heavy
381 isotopes associated with the coal organic matter will be preferentially released to the
382 vapor phase. Data sources: parent rock (Araújo et al. 2017; Bigalke et al. 2010;
383 Dolgopolova et al. 2006; Kříbek et al. 2016; Lv et al. 2016; Martin et al. 2018; Vance

et al. 2016; Viers et al. 2007; Xia et al. 2020); soil (Bigalke et al. 2013; Bigalke et al. 2010; Fekiacova et al. 2015; Kříbek et al. 2016; Lv et al. 2020; Sivry et al. 2008; Vance et al. 2016; Viers et al. 2007; Xia et al. 2020); ore (Aebischer et al. 2015; Araújo et al. 2017; Deng et al. 2017; Dolgopolova et al. 2006; Kříbek et al. 2016; Maréchal et al. 1999; Martin et al. 2018; Mason et al. 2005; Matt et al. 2020; Mattielli et al. 2009; Mondillo et al. 2018; Sivry et al. 2008; Xia et al. 2020); smelting (Araújo et al. 2018; Bigalke et al. 2010; Martin et al. 2018; Mattielli et al. 2009; Yin et al. 2018); raw coal (Borrok et al. 2010; Gonzalez and Weiss 2015); fly ash (Gonzalez and Weiss 2015; Sivry et al. 2008); bottom ash (Borrok et al. 2010; Gonzalez and Weiss 2015); fertilizer (Chen et al. 2008; Xia et al. 2020); sewage sludge (Chen et al. 2008); traffic activities (Cloquet et al. 2006a; Dong et al. 2017); waste incineration (Cloquet et al. 2006a; Martin et al. 2018).

3.4 Strontium (Z = 38)

Strontium (Sr) has four stable isotopes, ^{84}Sr (0.6%), ^{86}Sr (9.9%), ^{87}Sr (7.0%), and ^{88}Sr (82.6%) (Hoefs 2018). One isotope (^{87}Sr) is influenced by radiogenic processes, while the others (^{84}Sr, ^{86}Sr and ^{88}Sr) are only affected by fractionation (Bullen 2014; Wiederhold 2015). The standard reference material for Sr isotope ratios is NIST SRM 987 (Hoefs 2018; Wang et al. 2019c), but different to the non-radiogenic metals, the isotope ratios of partly radiogenic elements are not given in the delta notation but as ratios. This has historic reasons and is also attributable to the fact that the Sr isotope

405 ratios are sufficiently distinct among different materials.

406 Variations in Sr isotopes (i.e., the $^{87}Sr/^{86}Sr$ ratio) are induced both by radiogenic
407 processes (^{87}Rb-^{87}Sr beta decay, half-life 48.8 billion years) and isotope fractionation
408 (e.g., carbonate precipitation) (Sherman et al. 2015; Wiederhold 2015). Different ages,
409 lithology and geochemical compositions of the source materials, as well as various
410 hydrological processes (e.g., precipitation and dissolution) result in discernible
411 variations of Sr isotopic signatures among environmental samples (Bullen 2014; Hoefs
412 2018; Wang et al. 2020e; Wiederhold 2015) (Table 1). Current findings suggest that
413 fertilizers, irrigation waters, and urban emissions share similar $^{87}Sr/^{86}Sr$ ratios, while
414 pesticides, ores and coal fly ash samples are isotopically heavier (Table 1). The
415 relatively subtle intra-source variations (presented as the standard deviation in Table
416 1) favor the source identification, which is, however, in some circumstances,
417 compensated by overlapped inter-source $^{87}Sr/^{86}Sr$ isotopic signatures (Table 1). For
418 instance, fertilizers, vehicle exhausts and solid wastes usually possess similar isotopic
419 signatures.

420 Strontium isotope analysis has nevertheless been successfully employed in soil metal
421 source apportionment (Ayuso and Foley 2018; Erel and Torrent 2010; Kong et al. 2018;
422 Li et al. 2016). For instance, Sun et al. (2017) have found that the concentration of Sr
423 in soil samples collected along a highway correlated well with the $^{87}Sr/^{86}Sr$ ratio ($p <$
424 0.01), indicating that the Sr isotope ratio is mainly controlled by the mixing sources of
425 parent material and vehicle emissions (unpolluted soils has lower Sr concentrations

and higher $^{87}Sr/^{86}Sr$ ratios, while contaminated soils enriched by anthropogenic Sr has lower $^{87}Sr/^{86}Sr$ ratios). To overcome the problems with not sufficiently distinct source signals of Sr isotope ratios, Sr isotopes are frequently analyzed together with Pb isotopes for the quantitative identification of multi-sources. Because both Sr and Pb isotopes ratios are partly caused by radioactive decay (Section 3.8), results from both approaches often corroborate each other (Du et al. 2017; Lin et al. 2016; Sun et al. 2018; Tan et al. 2017).

Table 1 The $^{87}Sr/^{86}Sr$ ratios of different samples as a result of radioactive decay and isotope fractionation.

Sample	$^{87}Sr/^{86}Sr$ (mean ± SD)	References
Agricultural sources		
Fertilizer (n=27)	0.709 ± 0.002	(Ayuso and Foley 2018; Delattre et al. 2020; Hosono et al. 2007; Kume et al. 2010; Thomsen and Andreasen 2019; Zieliński et al. 2016)
Irrigation water (n=10)	0.709 ± 0.001	(Delattre et al. 2020; Hosono et al. 2007; Kume et al. 2010; Techer et al. 2017)
Pesticide (n=3)	0.727 ± 0.028	(Techer et al. 2017)
Industrial sources		
Fly ash (n=65)	0.713 ± 0.004	(Hurst and Davis 1981; Hurst et al. 1991; Lin et al. 2016; Ruhl et al. 2014; Wang et al. 2019c; Wang et al. 2020e; Widory et al. 2010)
Ore (n=8)	0.716 ± 0.007	(Lin et al. 2016; Tan et al. 2017)
Smelting (n=2)	0.711 ± 0.002	(Geagea et al. 2008; Widory et al. 2010)
Cement production (n=6)	0.710 ± 0.001	(Geagea et al. 2008; Wang et al. 2019c; Widory et al. 2010)
Urban sources		
Traffic emission (n=11)	0.710 ± 0.001	(Geagea et al. 2008; Lin et al. 2016; Wang et al. 2019c)
Solid waste (n=10)	0.709 ± 0.001	(Geagea et al. 2008; Wang et al.

2019c)

3.5 Cadmium (Z = 48)

Cadmium has eight stable isotopes: ^{106}Cd (1.2%), ^{108}Cd (0.9%), ^{110}Cd (12.5%), ^{111}Cd (12.8%), ^{112}Cd (24.1%), ^{113}Cd (12.2%), ^{114}Cd (28.7%), and ^{116}Cd (7.5%) (Hoefs 2018). The $\delta^{114/110}Cd$ value is often adopted to depict Cd isotope variations (Eq. 21):

$$\delta^{114/110}Cd = \left(\frac{(^{114}Cd/^{110}Cd)_{sample}}{(^{114}Cd/^{110}Cd)_{standard}} - 1\right) \times 1000 \quad (21)$$

NIST SRM 3108 is the commonly used reference material for this element (Hoefs 2018).

Variations in Cd isotopes are largely governed by two major processes, namely evaporation/condensation and biological activities (Barraza et al. 2019; Hoefs 2018; Salmanzadeh et al. 2017). Since Cd isotopes fractionate during evaporation/condensation, detectable isotope fractionation will occur during coal combustion and metal smelting (Fouskas et al. 2018; Gao et al. 2013; Hoefs 2018) (Figure 3, all isotope ratios are converted to $\delta^{114/110}Cd_{NIST\ 3108}$). Results from two coal-fired power plants in US suggest that heavier Cd isotopes will be enriched in fly ash than in bottom ash during coal combustion (Fouskas et al. 2018). This is because heavier isotopes will be preferentially condensed onto fine fly ash particles during flue gas cooling (Fouskas et al. 2018) (Figure 3). During metal smelting and refining, significant enrichment of heavier Cd isotopes in the products is observed relative to the starting materials ($\delta^{114/110}Cd_{PCIGR-1}$ shifted from -0.13‰ ~ +0.18‰ to +0.39‰ ~ +0.52‰ after roasting, sulfide leaching and purification), which is because lighter

457 isotopes are preferentially released to the flue gas during evaporation (>900 °C) and
458 emitted to the atmosphere (Shiel et al. 2010). It is noteworthy that the fractionation
459 patterns of Cd and Zn are quite similar during evaporation-condensation. For coal
460 combustion, heavier isotopes would enrich in fly ash (Fouskas et al. 2018; Gonzalez
461 and Weiss 2015). However, for metal smelting, heavier ones would retain in products
462 (Mattielli et al. 2009; Shiel et al. 2010). The underlying mechanisms should be further
463 explored.

464 Biological activities will lead to the preferential enrichment of heavier or lighter isotopes
465 in organisms. Heavier Cd isotope compositions than in bulk soil were observed in pod
466 husks and leaves of cacao beans (Barraza et al. 2019). A recent study by Zhou et al.
467 (2020) found that the Cd hyperaccumulator *S. plumbizincicola* tended to accumulate
468 heavier Cd during repeated phytoextraction due to the presence of specific Cd
469 transporter proteins. However, for the Cd hyperaccumulator *Solanum nigrum* L. and
470 Cd-tolerant non-hyperaccumulator *Ricinus communis* L. a reverse trend was observed,
471 with both plants tending to accumulate lighter Cd relative to a hydroponic solution (Wei
472 et al. 2018). The finding that wheat (*Triticum aestivum* L.) and barley plants (*Hordeum*
473 *vulgare* L.) showed a heavier Cd isotope ratio than the bulk soil but a lighter or similar
474 one than the plant-available $Ca(NO_3)_2$-extractable pool or the soil solution (Imseng et
475 al. 2019a; Wiggenhauser et al. 2019), reconciles the above apparently contradicting
476 results. Retranslocation of Cd in plants from roots to shoots and grains of wheat and
477 barley, and from roots to stems and leaves of *S. nigrum* favored the heavy Cd isotopes

478 (Imseng et al. 2019a; Wei et al. 2018; Wiggenhauser et al. 2019), while the plant-
479 internal stable Cd isotope fractionation in *R. communis* showed variable fractionation
480 directions (Wei et al. 2018), possibly due to different plant strategies to cope with Cd.
481
482 Cadmium isotopes can be powerful indicators of industrial sources (Figure 6). Wang
483 et al. (2019b) found that Cd isotope compositions for agricultural soils collected from
484 the Jianghan Plain, China were similar with those for smelter dust and incinerator fly
485 ash, indicating that industrial origins, such as smelting and refining processes are the
486 major Cd sources. This finding was corroborated by traditional source apportionment
487 strategies, such as Pb isotope analysis and statistical analysis approaches. Wen et al.
488 (2015) analyzed Cd isotope signatures in a typical Pb-Zn mining area in China, and
489 found that compared with unpolluted soils ($\delta^{114/110}Cd_{Spex} > 0$), isotopes in Cd-
490 enriched soils in the vicinity of the Pb-Zn mine were lighter ($\delta^{114/110}Cd_{Spex} < 0$). Apart
491 from industrial sources, comparison of Cd isotope signatures between phosphate
492 fertilizers and the agricultural soils may also provide information on agricultural activity-
493 dominated Cd accumulation (Salmanzadeh et al. 2017), but the variability of Cd
494 isotopic signatures within the agricultural sources may not be sufficiently distinct
495 (Figure 3). Furthermore, the intra-source low-temperature Cd isotope fractionation,
496 such as the biological MDF (Barraza et al. 2019) and adsorption to soil minerals or
497 organic matter (Chrastný et al. 2015) will add difficulty to source identification, since
498 the redistribution of soil Cd isotope signals may overlap with the distinct Cd isotope

signatures of the external input (i.e., industrial sources) (Figure 3, relatively large variations have been observed for soil samples).

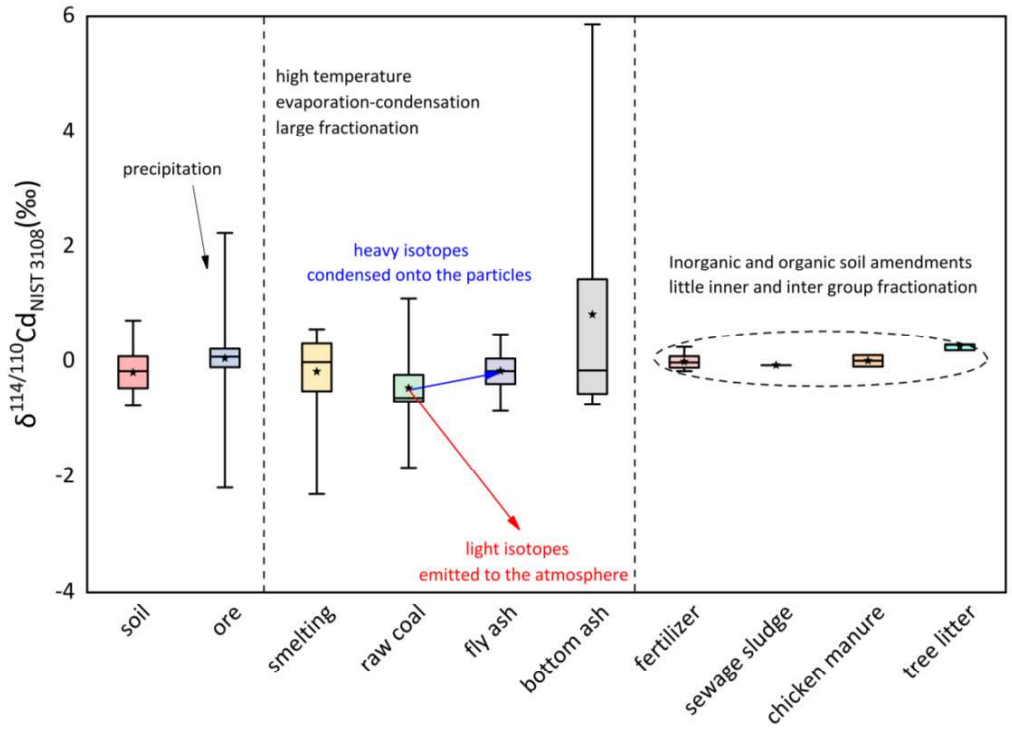

Figure 3 Cd isotope fractionation of environmental samples. All isotope ratios are converted to $\delta^{114/110}Cd_{NIST\ 3108}$. Evaporation-condensation and the mineral precipitation during ore formation result in large variations in $\delta^{114/110}Cd$ ratios. In comparison, isotopic signatures of agriculture sources are not distinct enough. Data sources: soil (Barraza et al. 2019; Chrastný et al. 2015; Cloquet et al. 2006b; Imseng et al. 2018; Pallavicini et al. 2014; Salmanzadeh et al. 2017; Wang et al. 2019b; Wen et al. 2015); ore (Chrastný et al. 2015; Gao et al. 2013; Liu et al. 2020c; Martinková et al. 2016; Shiel et al. 2010; Wang et al. 2020a; Wen et al. 2015; Xu et al. 2020; Zhu et al. 2016; Zhu et al. 2017); smelting (Chrastný et al. 2015; Cloquet et al. 2006b; Martinková et al. 2016; Shiel et al. 2010; Wen et al. 2015); raw coal (Fouskas et al.

2018; Martinková et al. 2016); fly ash (Chrastný et al. 2015; Fouskas et al. 2018; Martinková et al. 2016); bottom ash (Fouskas et al. 2018; Martinková et al. 2016); fertilizer (Imseng et al. 2018; Salmanzadeh et al. 2017); sewage sludge (Pallavicini et al. 2014); chicken manure (Barraza et al. 2019); tree litter (Barraza et al. 2019).

3.6 Mercury (Z = 80)

There are seven stable mercury isotopes, ^{196}Hg (0.2%), ^{198}Hg (10.0%), ^{199}Hg (16.9%), ^{200}Hg (23.1%), ^{201}Hg (13.2%), ^{202}Hg (29.9%) and ^{204}Hg (6.9%) (Hoefs 2018). Because ^{198}Hg is the isotope with the lowest mass that can still be precisely measured, and ^{202}Hg is that with the highest mass which is free of isobaric interferences (Blum et al. 2014; Yin et al. 2014), MDF-induced mercury isotope variations are often reported as the $\delta^{202/198}Hg$ value (Eq. 22):

$$\delta^{202/198}Hg = \left(\frac{(^{202}Hg/^{198}Hg)_{sample}}{(^{202}Hg/^{198}Hg)_{standard}} - 1\right) \times 1000 \quad (22)$$

The internationally used reference material is NIST SRM 3133 (Hoefs 2018; Rumble et al. 2018; Yin et al. 2014).

In addition to MDF, large MIF has been observed for Hg. The MIF of Hg isotopes is usually expressed as the difference between the measured $\delta^{202/198}Hg$ value and that theoretically-predicted assuming only MDF (Eq. 23-26) (Blum et al. 2014; Hoefs 2018):

$$\Delta^{199}Hg = \delta^{199/198}Hg - \left(\delta^{202/198}Hg \times 0.2520\right) \quad (23)$$

$$\Delta^{200}Hg = \delta^{200/198}Hg - \left(\delta^{202/198}Hg \times 0.5024\right) \quad (24)$$

$$\Delta^{201}Hg = \delta^{201/198}Hg - \left(\delta^{202/198}Hg \times 0.7520\right) \quad (25)$$

533 $$\Delta^{204}Hg = \delta^{204/198}Hg - \left(\delta^{202/198}Hg \times 1.4930\right) \quad (26)$$

534 There are three types of Hg isotope fractionation. Firstly, MDF occurs in all biotic and
535 abiotic reactions during the biogeochemical cycle of Hg, such as adsorption (Jiskra et
536 al. 2012), methylation/demethylation (Jiménez-Moreno et al. 2013), and evaporation
537 (Ghosh et al. 2013) (Figure 4). Secondly, the odd-MIF (reported as the $\Delta^{199}Hg/\Delta^{201}Hg$
538 ratio) occurs during the photochemical reduction of divalent mercury [Hg(II)] to
539 methylmercury (MeHg) and the evaporation of elemental mercury [Hg(0)] (liquid-vapor
540 transition). Furthermore, even-MIF (reported as the $\Delta^{200}Hg/\Delta^{204}Hg$ ratio) is related
541 to the photochemical oxidation of Hg(0) in the atmosphere (Blum and Johnson 2017;
542 Hoefs 2018; Yin et al. 2014).

543 Coal combustion is the major source of anthropogenic Hg emissions into the
544 environment, accounting for 21% of the annual Hg emissions (UNEP 2018). As shown
545 in Figure 4, the $\delta^{202/198}Hg_{NIST\ 3133}$ value of raw coal samples vary greatly from -3.9‰
546 to +0.8‰. Current studies suggest that lighter Hg isotopes will volatize more easily in
547 the coal-fired boilers, resulting in isotopically lighter Hg compositions in the fly ash
548 ($\delta^{202/198}Hg_{NIST\ 3133}$= -1.3‰ ± +0.5‰) relative to the raw coal (-1.2‰ ± +0.8‰).
549 Correspondingly, the residual Hg in the bottom ash is enriched in heavier isotopes (-
550 1.0‰ ± 0.9‰) (Huang et al. 2017; Sun 2019; Sun et al. 2014a; Tang et al. 2017) (Figure
551 4). Apart from coal combustion, it is hypothesized that other high-temperature
552 industrial processes, such as cement production, metal smelting and waste
553 incineration will also lead to significant MDF. Unlike the large MDF signatures of Hg

among various samples ($\delta^{202/198}Hg_{NIST\ 3133}$= -4.4‰ ~ +2.1‰), most of the land-based samples (e.g., rocks and ores) reveal little MIF ($\Delta^{199}Hg$ =-0.2‰ ~ +0.6‰) (Figure 4). In comparison, large MIF is observed in rainwater and snow samples, suggesting that the atmospheric photochemical reactions dominate the mass-independent fractionation of this element (Chen et al. 2012; Sherman et al. 2010) (Figure 4).

Both MDF and MIF can be used for the source identification of Hg (Figure 6). The MDF signatures are important indicators for local industrial sources (e.g., mining, smelting, coal combustion), while MIF indicates the long-range atmospheric transport of this contaminant. Estrade et al. (2011) found that the $\delta^{202/198}Hg_{NIST\ 3133}$ values of the contaminated top soils in the vicinity of a metal smelter fell between those of the atmospheric deposition and the geogenic background. Moreover, the $\delta^{202/198}Hg_{NIST\ 3133}$ values correlated closely with the inverse of the Hg concentrations 1/[Hg] ([Hg] represents the Hg concentrations in samples) (r=0.89), indicating a mixing between geogenic Hg and local anthropogenic Hg (the severer the contamination is, the heavier the isotope will be detected). Yin et al. (2013a) found an interesting phenomenon, that the variation of MIF ($\Delta^{199}Hg$) in wheat tissues grown in a mining affected region revealed a mixing between atmospheric and soil Hg. The MIF followed the order of air (-0.30‰) < leaf (-0.25‰) < stem (-0.15‰) < root (-0.04‰) < soil (0). This indicated that the roots took up Hg exclusively from soil (no MIF), while the aboveground tissues also accumulated Hg directly from the atmosphere (negative MIF). Feng et al. (2013) examined both MDF and MIF in surface soils collected either

575 from Wanshan Mercury Mine, the “mercury capital” in China where Hg mining activities
576 have lasted for more than 3000 years (soil Hg concentration 49 ~ 127 mg kg^{-1}), or from
577 a control site with no direct point contamination source of Hg (soil Hg concentration
578 0.25 ~ 0.30 mg kg^{-1}). The $\delta^{202/198}Hg_{NIST\ 3133}$ values of soil samples from the mining
579 area fell in between the local Hg waste calcine and Hg ore samples while no
580 statistically significant MIF was observed (p > 0.2), which suggested that local sources
581 played a major role. In comparison, the Hg isotope signatures of the control site
582 revealed detectable MIF, indicating that atmospheric deposition after long-range
583 transport was a source of Hg in this area (Figure 6).

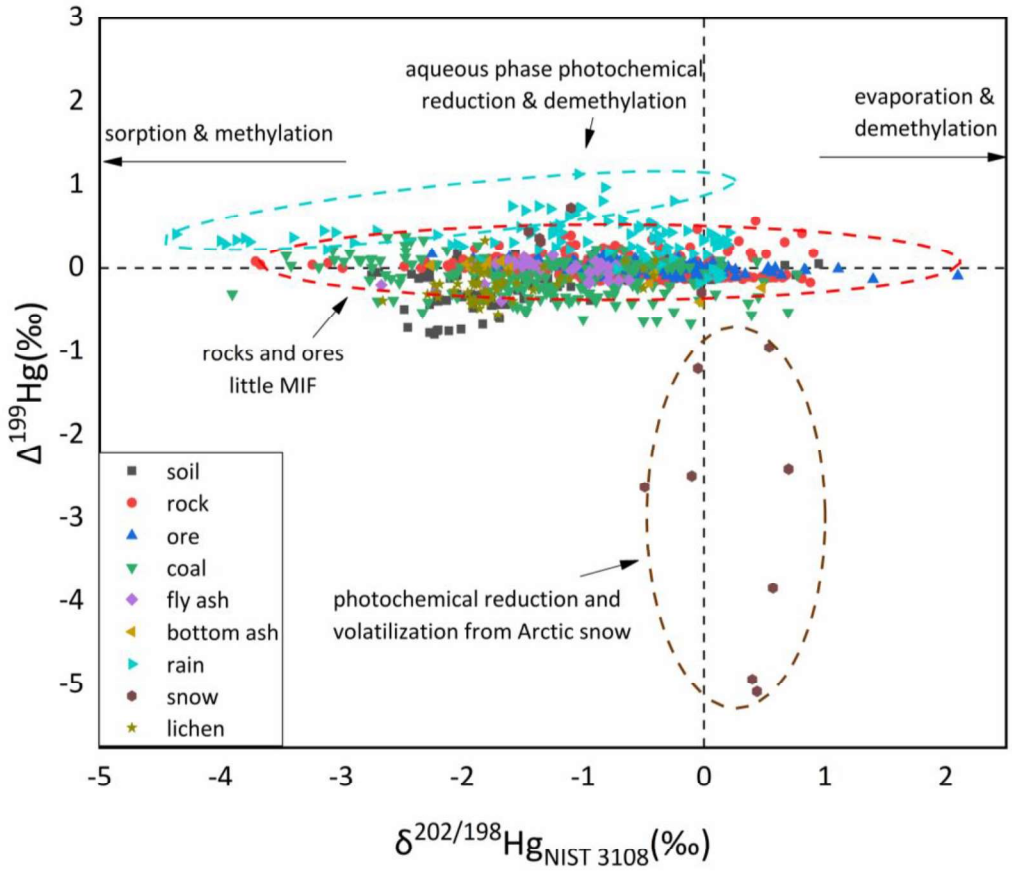

584

585 Figure 4 Representation of various environmental samples in the dual isotope space

586 of Hg. All isotope ratios are reported relative to NIST SRM 3133. The
587 $\delta^{202/198}Hg_{NIST\,3133}$ value is used to represent mass-dependent isotope fractionation
588 of Hg (MDF), while the $\Delta^{199}Hg$ value (see Eq. 23 for its definition) is used to represent
589 mass-independent isotope fractionation of Hg (MIF). Hg isotope signatures resulting
590 from MDF are common in all samples, while Hg isotope signatures resulting from MIF
591 only occur in samples of atmospheric origin. Positive MIF as a result of photochemical
592 reduction and demethylation in the aqueous phase is observed in rainfall samples
593 (Blum et al. 2014; Gratz et al. 2010; Yuan et al. 2018). Large negative MIF is observed
594 in Arctic snow samples because of the preferential photochemical reduction of odd
595 isotopes to Hg(0). As a result, the residual Hg(II) in the snowpack reveals highly
596 negative $\Delta^{199}Hg$ values (Sherman et al. 2010). Data sources: soil (Baptista-Salazar
597 et al. 2018; Biswas et al. 2008; Blum et al. 2014; Feng et al. 2010; Goix et al. 2019;
598 Gray et al. 2013; Jiskra et al. 2017; Pribil et al. 2020; Yin et al. 2013a; Yin et al. 2020;
599 Zhang et al. 2020a); rock (Blum et al. 2014; Smith et al. 2008; Yin et al. 2019; Zerkle
600 et al. 2020; Zhang et al. 2020a); ore (Baptista-Salazar et al. 2018; Blum et al. 2014;
601 Feng et al. 2010; Gray et al. 2013; Jiménez-Moreno et al. 2016; Pribil et al. 2020;
602 Schudel et al. 2019; Wiederhold et al. 2013; Yin et al. 2013b); coal (Biswas et al. 2008;
603 Feng et al. 2010; Huang et al. 2017; Sherman et al. 2012; Sun 2019; Sun et al. 2014a;
604 Sun et al. 2014b; Tang et al. 2017); fly ash (Huang et al. 2017; Sun 2019; Sun et al.
605 2014a; Tang et al. 2017); bottom ash (Huang et al. 2017; Sun 2019; Tang et al. 2017);
606 rain (Blum et al. 2014; Chen et al. 2012; Gratz et al. 2010; Sherman et al. 2012; Yuan

et al. 2018); snow (Chen et al. 2012; Sherman et al. 2010); lichen (Blum et al. 2014; Jiménez-Moreno et al. 2016; Yin et al. 2013a).

3.7 Thallium (Z = 81)

Thallium has two stable isotopes, ^{203}Tl (29.5%) and ^{205}Tl (70.5%) (Hoefs 2018). The Tl isotope variations are usually reported as the $\varepsilon^{205}Tl$ value (Eq. 27):

$$\varepsilon^{205}Tl = \left(\frac{(^{205}Tl/^{203}Tl)_{sample}}{(^{205}Tl/^{203}Tl)_{standard}} - 1\right) \times 10000 \quad (27)$$

The generally used reference material is NIST SRM 997 (Hoefs 2018).

The processes responsible for the variations in Tl isotopes are still under debate. Evaporation/condensation processes are possibly the major causes of Tl isotope fractionation (Liu et al. 2020b; Vanek et al. 2016) (Figure 5). Limited evidence has shown that Tl isotope analysis can be applied for source apportionment. Kersten et al. (2014) observed that the topsoil in the vicinity of a cement plant was enriched by heavier Tl isotopes ($\varepsilon^{205}Tl_{NIST\ 997} = 0$), while the deep soils was isotopically lighter ($\varepsilon^{205}Tl_{NIST\ 997} = -4$) (Figure 5). The $\varepsilon^{205}Tl_{NIST\ 997}$ value of the cement kiln dust was the same as that of top soils, indicating that historical Tl emissions from the cement production resulted in soil contamination. Vaněk et al. (2018) found that $\varepsilon^{205}Tl_{NIST\ 997}$ values for surface soils (O horizon) affected by mining and smelting activities (-3.92 ~ -2.69) were similar with those of ore (-3.76), slag (-3.31) and other industrial waste samples (-4.77 ~ -3.60), while uncontaminated deep soil samples (C horizon) were isotopically lighter (-2.71 ~ -0.41) (Figure 5). The small variation of the Tl isotopic

628 composition (usually < 1‰, Figure 5) currently limits its use for source attribution, at
629 least until analytical procedures have advanced so far that the precision is sufficient to
630 disentangle differences in isotope signals in the sub-permil area.

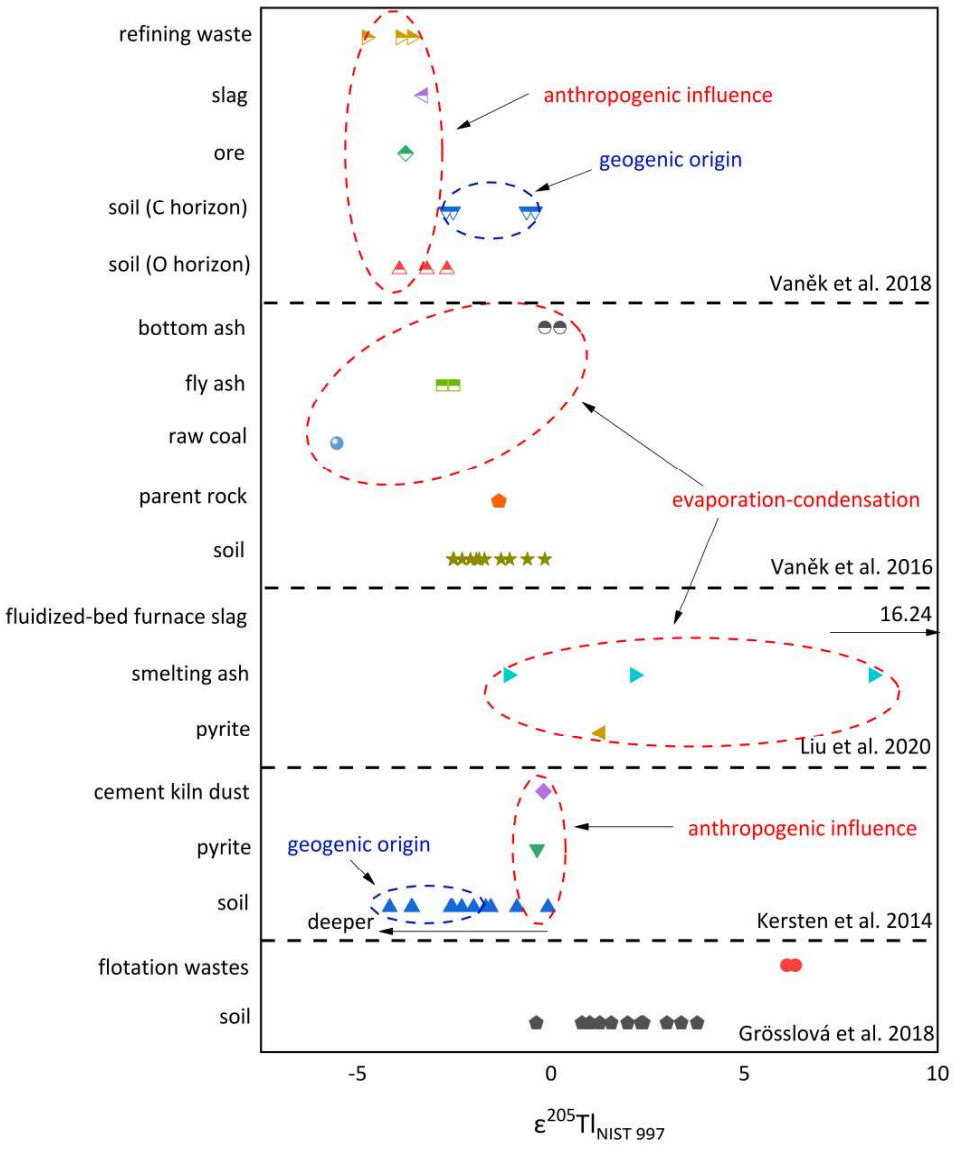

631

632 Figure 5 Stable Tl isotope ratios in environmental samples. All isotope ratios are
633 reported relative to NIST SRM 997. Evaporation-condensation is believed to be a

major cause of Tl isotope fractionation. Current studies suggest that Tl isotopes can be used to identify the influence of coal combustion, cement production, metal smelting and other industrial sources. Data sources: (Grösslová et al. 2018; Kersten et al. 2014; Liu et al. 2020b; Vaněk et al. 2018; Vanek et al. 2016).

3.8 Lead (Z = 82)

Pb is present in nature in the form of four stable isotopes: ^{204}Pb (1.4%), ^{206}Pb (24.1%), ^{207}Pb (22.1%) and ^{208}Pb (52.4%) (Cheema et al. 2020; Rumble et al. 2018). ^{204}Pb is the only primitive stable isotope formed in the big bang, while ^{206}Pb, ^{207}Pb and ^{208}Pb are radioactive decay products of ^{238}U, ^{235}U and ^{232}Th, respectively (Eq. 28-30):

$$^{238}_{92}U \rightarrow {}^{206}_{82}Pb + 8\alpha + 6\beta^- + Q \quad (28)$$

$$^{235}_{92}U \rightarrow {}^{207}_{82}Pb + 7\alpha + 4\beta^- + Q \quad (29)$$

$$^{232}_{90}Th \rightarrow {}^{208}_{82}Pb + 6\alpha + 4\beta^- + Q \quad (30)$$

where α represents the alpha particle, β^- refers to the beta particle, Q is the energy released during the decay. The decay rates are extremely slow (half-life $4.468 \times 10^9, 7.038 \times 10^8,\ 1.401 \times 10^{10}$ years for Eq. 28, 29 and 30, respectively) (Cheema et al. 2020; Cheng and Hu 2010; Schoene 2014). Lead isotope compositions are usually reported as the ^{206}Pb/^{204}Pb, ^{206}Pb/^{207}Pb and ^{208}Pb/^{206}Pb ratios, while ^{206}Pb/^{207}Pb and ^{208}Pb/^{206}Pb are preferred. Because of the high abundance of ^{206}Pb, ^{207}Pb and ^{208}Pb, ratios among these three isotopes can be precisely detected even with an ICP-QMS (typical measurement precision 0.1% ~ 0.5%) (Cheema et al. 2020; Cheng and Hu 2010). The reference material for Pb isotopes is the NIST SRM 981.

Compared with other metal isotopes whose variations are mainly induced by fractionation, up to now the subtle Pb isotope fractionation during industrial and environmental processes has not yet been fully acknowledged (Figure 6). Instead, stable isotope variations of Pb are attributed to radioactive decay (Schoene 2014; Wiederhold 2015). Depending on the age and the geochemical composition of the source materials, large Pb isotope variations have been observed among environmental samples. Lead isotopes have been extensively applied for source apportionment purposes. Traffic activities (in the time of widely used leaded gasoline, which phases out since the end of the 20th century) (Kelepertzis et al. 2016; Peng et al. 2020), coal combustion (Bińczycki et al. 2020; Chen et al. 2019), metal smelting (Kelepertzis et al. 2020; Lee et al. 2020b), mining activities (Wang et al. 2019a), e-waste processing (Jiang et al. 2019), irrigation & fertilization (Liu et al. 2019a) and natural weathering (Jia et al. 2020a; Wen et al. 2020) can be primary sources of Pb accumulation in soils. Lead isotope analysis may also shed light on the source identification of multi-elements (Section 4). For a detailed discussion of source apportionment using Pb isotopes, readers are referred to Cheema et al. (2020), Cheng and Hu (2010) and Komarek et al. (2008), who have provided comprehensive overviews of this topic.

3.9 Non-metallic elements

Stable isotopes of non-metallic elements (e.g., C, N, O, S) (also termed as traditional stable isotopes) can aid in metal source apportionment in an indirect way. Morera-

Gómez et al. (2020) analyzed $\delta^{13}C$ and $\delta^{15}N$ values, as well as metal concentrations of urban road dust samples collected in Cienfuegos, Cuba. Based on the results from the cluster analysis that takes both metal concentrations and the isotope ratios into account, sampling sites were divided into four categories with distinct major pollution sources. The role of the $\delta^{13}C$ value was to reveal the contribution of carbonates (that can be related to industrial emissions such as cement production), while the $\delta^{15}N$ value reflected the contribution of particulate organic matter (Morera-Gómez et al. 2020). Sulfur isotope ratios can be useful indicators of metal sulfide (e.g., CuS, ZnS, PbS) oxidation, a main process contributing to the release of metals (oxidized samples have higher $\delta^{34}S$ values). Dótor-Almazán et al. (2017) found that mineral oxidation in mine tailing samples increased following the order of galena (PbS) < chalcopyrite (CuS) < sphalerite (ZnS), indicating that mine tailings are more likely to cause Zn and Cu than Pb contamination of the adjacent soil and river. Cui et al. (2014) observed significant positive correlations between $\delta^{34}S$ values and Cd concentrations (p < 0.01) and between $\delta^{34}S$ values and Pb concentrations in the river sediment (p < 0.01). The authors explained this finding by the fact that Cd and Pb mainly occurred in the form of sulfides in the studied samples and concluded that, sulfur isotope ratios may be a reliable indicator of metal contamination in the sediment. Furthermore, $\delta^{34}S$ values of the sediment samples (+2.64‰) fell in between natural bedrock (+8.9‰) and metal ores (+0.28‰), which enabled the quantitative source apportionment. Kim et al. (2020) observed increasing

697 $\delta^{18}O_{SO4}$ values (in sulfate) with increasing mineral oxidation and dissolution in
698 groundwater samples collected from a metalliferous mining area. In addition, the Zn/Cd
699 ratio of the adjacent soil approached those of groundwater samples and was different
700 from that of the surrounding mine tailings, which suggests that metals from mine
701 tailings may have first entered the groundwater aquifer, and then contaminated the
702 soils indirectly.
703
704
705

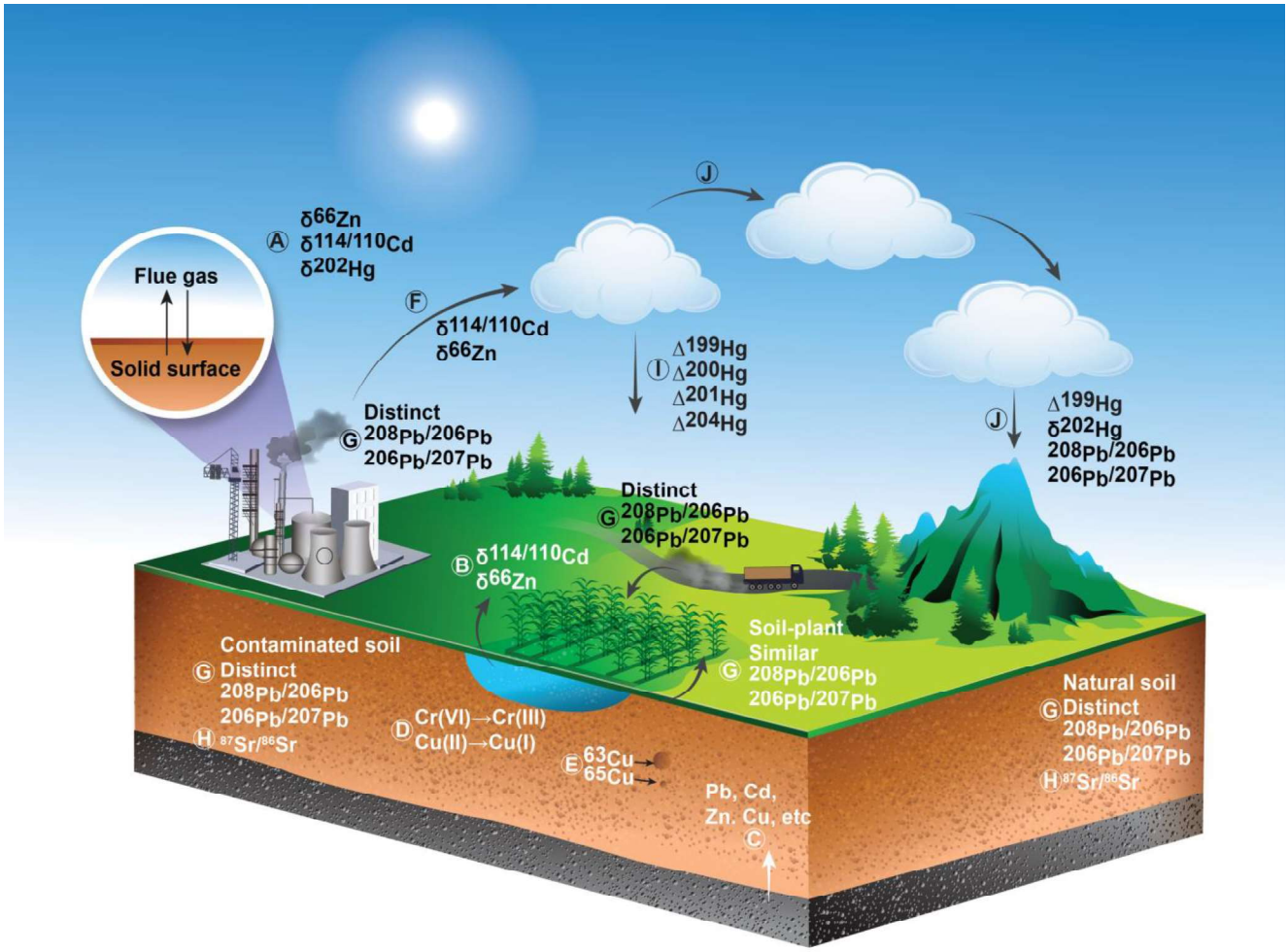

707 Figure 6 Overview of the reviewed stable isotope systems that can potentially be used
708 for the source apportionment of soil metals. (A) Mass-dependent fractionation (MDF)
709 occurs during evaporation/condensation processes (Hoefs 2018; Wiederhold 2015).
710 (B) MDF by biological processes (membrane transport, complexation, xylem/phloem
711 transport, element storage and retranslocation) results in the preferential uptake of
712 isotopes (Hoefs 2018; Wiederhold 2015). (C) In soils without anthropogenic
713 disturbance, the dominant source of metals is the parent rock of soil formation (Alloway
714 2013). (D) The redox processes of Cr and Cu result in substantial MDF that would add

715 difficulty to source tracing but favor process tracing (Berna et al. 2010; Markl et al.
716 2006). (E) Preferential sorption of Cu isotopes onto soil minerals can lead to low-
717 temperature isotope fractionation (Babcsanyi et al. 2016; Li et al. 2015). (F) Zn and Cd
718 isotopes are particularly useful for the source apportionment of smelting and
719 combustion-induced soil contamination (Li et al. 2019; Wang et al. 2019b). (G) In-situ
720 fractionation by biogeochemical processes seems negligible for Pb isotopes. Distinct
721 Pb isotope compositions amongst environmental samples with different geochemical
722 compositions enable the quantitative source apportionment (Cheng and Hu 2010;
723 Wiederhold 2015). (H) Sr isotopes are usually analyzed together with Pb isotopes for
724 the quantitative identification of multi-sources (Sun et al. 2018; Zhao et al. 2019a). (I)
725 Mass-independent fractionation (MIF) induced by photochemical reactions can reveal
726 the atmospheric origin of Hg (Blum et al. 2014; Hoefs 2018). (J) Long-range transport
727 and atmospheric deposition can be dominant sources of metals in remote areas (Bing
728 et al. 2014; Feng et al. 2013).
729

730 # 4 Source identification of multi-metal contaminated soils

731 Because of the high cost and complicated pre-treatment procedures for a stable
732 isotope analysis, most studies have selected isotopes of a single element for the
733 source apportionment of soil metals. However, soils are often contaminated by multi-
734 elements with different main sources (Chen et al. 2015; Luo et al. 2012; Tong et al.
735 2020; Xiao et al. 2020; Xie et al. 2019). For instance, atmospheric deposition is often

736 regarded as a major source of Hg due to its high volatility (Driscoll et al. 2013; UNEP
737 2018), rock weathering contribute greatly to soil Cd accumulation (especially in
738 southwest China) (Gong et al. 2020; Luo and Teng 2018), while mining & smelting are
739 often found to be the major source of soil Pb (Cheema et al. 2020; Zhang et al. 2019b).
740 How to reveal the sources of each metal in such soils with the help of the selected
741 isotopes remains a tough challenge in terms of cost and labor.
742 Several attempts have been made to seek for strategies for multi-metal source
743 apportionment. A combination of Pb isotope analysis and statistical or mineralogical
744 analysis approaches have proven to be helpful for the source identification of multi-
745 metals in soil (Table 2). Several studies have observed a strong positive correlation
746 between Pb and other metals, which suggested that these metals may share similar
747 origins (Huang et al. 2020; Liu et al. 2016). Based on the correlation analysis result,
748 quantitative source apportionment were conducted using Pb isotopes (Huang et al.
749 2020; Liu et al. 2016; Liu et al. 2020a) (Table 2). However, this method is criticized
750 because of the lack of direct evidence. Other studies have simultaneously investigated
751 the mineralogy as well as stable isotope ratios (Table 2). An in-depth investigation of
752 metal speciation provides much stronger support for the extrapolation of Pb isotope
753 analysis results to other metals. For instance, Jeon et al. (2017) found that X-ray
754 diffraction (XRD) results corroborated well with the Pb isotope-based source
755 apportionment, that Zn smelting was the major source of metal accumulation in the
756 studied region. Because of sulfide oxidation, geogenic ZnS is unlikely to be present in

757 soil in the original form. However, sphalerite (ZnS) was observed in fine soil particles
758 (< 0.044 mm), indicating that anthropogenic sources contributed most to soil Zn
759 contamination. Lee et al. (2020a) combined XRD, transmission electron microscopy
760 (TEM) and selected area electron diffraction (SAED) analysis to examine the feasibility
761 of Pb isotopes for the quantitative source apportionment of the monoisotopic element
762 As. The XRD patterns showed that the only As-bearing mineral in smelter dust was the
763 Pb-containing beudantite [$PbFe_3(OH)_6SO_4AsO_4$], which was different from primary As-
764 bearing minerals (without Pb) in host rocks (arsenopyrite, FeAsS) as observed by TEM
765 and SAED, suggesting that Pb isotopes are suitable for the source tracking of smelter-
766 based As. On the one hand, researchers should bear in mind that the biogeochemistry
767 of different elements varies. On the other hand, extrapolating the results from a single
768 isotope analysis approach is time-saving and cost-efficient, particularly when there is
769 a burgeoning demand for source apportionment of soil metals. If conventional Pb
770 isotope analysis were extrapolated with care (e.g., through statistical analysis or
771 mineralogical approaches), the results may aid in wise decision of sustainable risk
772 containment and soil remediation successfully (Hou 2020).

773

774 Table 2 Strategies for the source identification of multi-elements using single metal
775 isotopes.

Contaminant	Strategy	Precision of isotope analysis	Description	Major sources	Reference
Cd, Pb	Pb isotope (MC-ICP-MS) +	$^{206}Pb/^{207}Pb$ analytical precision	Soil Pb and Cd concentrations revealed a strong positive correlation (R=0.89), indicating that these metals may share	Coal combustion (85%), using	(Huang et al. 2020)

	Correlation analysis	0.03% (2σ)	similar origins	binary mixing model	
Zn, Pb	Pb isotope (ICP-QMS) + Mineralogical analysis (XRD)	$^{206}Pb/^{207}Pb$ residual standard deviation 0.64%; $^{208}Pb/^{206}Pb$ residual standard deviation 0.13%	The Pb isotope source apportionment results were verified using XRD analysis, that ZnS from the smelting fly ash was observed in fine soil fraction (less than 0.044 mm)	Metal smelting (60% - 90%), using binary mixing model	(Jeon et al. 2017)
Zn, Pb	Pb isotope (TIMS) + Mineralogical analysis (XRD)	$^{206}Pb/^{207}Pb$ analytical precision 0.01% (2σ); $^{208}Pb/^{206}Pb$ analytical precision 0.03% (2σ)	Mineralogical analysis results indicated the co-presence of ZnS, PbS (not recommended, weak evidence)	Metal smelting (83%), using binary mixing model	(Kang et al. 2019)
As, Pb	Pb isotope (TIMS) + Mineralogical analysis (XRD, TEM and SAED)	$^{206}Pb/^{207}Pb$ analytical precision 0.01% (2σ); $^{208}Pb/^{206}Pb$ analytical precision 0.03% (2σ)	XRD patterns suggested that the only As-bearing mineral in smelter dust was the Pb-containing beudantite [$PbFe_3(OH)_6SO_4AsO_4$], which was different from primary As-bearing minerals in host rocks (arsenopyrite, FeAsS) as observed by TEM & SAED	Natural (rock weathering, 79%), using binary mixing model	(Lee et al. 2020a)
Tl, Pb	Pb isotope (MC-ICP-MS) + Correlation analysis	$^{206}Pb/^{207}Pb$ analytical precision 0.01% (2σ); $^{208}Pb/^{206}Pb$ analytical precision 0.03% (2σ)	Soil Pb and Tl concentrations revealed a strong positive correlation (R=0.92), indicating that these metals may share similar origins	Mining and roasting of the pyrite ore	(Liu et al. 2016)
Tl, Pb	Pb isotope (MC-ICP-MS) + Correlation analysis	$^{206}Pb/^{207}Pb$ analytical precision 0.01% (2σ); $^{208}Pb/^{206}Pb$ analytical	$^{206}Pb/^{207}Pb$ and Tl concentrations revealed a strong positive correlation (R=0.79), indicating that Pb and Tl may share similar origins	Pyrite mining and smelting (46% - 91% for different vegetables), using binary	(Liu et al. 2020a)

	precision 0.03% (2σ)	mixing model

Abbreviations: MC-ICP-MS – multi-collector inductively coupled plasma mass spectrometer; ICP-QMS – inductively coupled plasma quadrupole mass spectrometer; TIMS – thermal ionization mass spectrometer; XRD – X-ray diffraction; TEM – transmission electron microscopy; SAED – selected area electron diffraction.

5 Temporal evolution and the aging phenomenon

Direct analysis of isotope compositions between environmental samples provides information on the sources of metals (where are soil metals from), while long-term monitoring and soil profile analysis reveal insights into temporal trends of metal accumulation and sources. Long-term monitoring provides direct information on the variation of metal sources with time. For instance, Salmanzadeh et al. (2017) investigated the Cd isotope composition of soil samples and fertilizer samples collected over 66 years (1959 to 2015) in New Zealand. The dominant source of Cd in this system was determined to be fertilizer application before 2000 AD. In contrast, recent fertilizer application did not result in a marked Cd accumulation, which was probably because grazing-related fractionation of Cd isotopes modified the observed isotopic compositions. Another study by Tomasevic et al. (2013) monitored Pb isotopic ratios in leaves of the urban tree species *Aesculus hippocastanum* L. and *Tilia* spp. from 2002 to 2009. The $^{206}Pb/^{207}Pb$ ratio decreased throughout the observation period, which was attributed to the decrease of leaded gasoline use.

796 However, in many cases, long-term monitoring can be difficult or even impossible. In
797 such circumstances, soil profiles may provide valuable information regarding historical
798 events and can be used to reveal the temporal trend of anthropogenic activities.
799 Isotope compositions of deeper soils reveal historical anthropogenic activities, while
800 those of surface soil samples indicate the influence of more recent sources of metal
801 emissions, because of the low mobility of most metals. For instance, Dawson et al.
802 (2010) suggested that the high $^{206}Pb/^{207}Pb$ ratios in the surface-near soil may stem
803 from the utilization of leaded petroleum, while high $^{206}Pb/^{207}Pb$ ratios at depths of more
804 than 40 cm may result from more ancient mining activity. Weiss et al. (2007) found that
805 the $\delta^{66}Zn_{JMC-Lyon}$ values of the top peat profile (+0.32‰ ~ +0.64‰ for soils <20 cm)
806 (formed during 1953~1997 AD as derived from ^{210}Pb and ^{14}C measurements) were
807 similar with those of the ore minerals (+0.10‰ ~ +0.50‰), suggesting historical mining
808 activities in the 20th century resulted in soil Zn contamination. In comparison, deeper
809 soils are isotopically heavier ($\delta^{66}Zn_{JMC-Lyon}$ fell within +0.99‰ ~ +1.43‰ for soils >60
810 cm) (1017~1192 AD), suggesting that the soils were unaffected by human activities at
811 ancient times.
812 Analysis of isotope compositions between different geochemical fractions of metals as
813 assessed with sequential extraction methods such as the Community Bureau of
814 Reference (BCR) (Quevauviller et al. 1993) or Tessier method (Tessier et al. 1979) can
815 also provide much information on the temporal trend of metal accumulation. Metals
816 exist in soils as different geochemical fractions, which is also affected by immobilizing

reagents and their aging processes (Hou et al. 2020b; Wang et al. 2020c; Wang et al. 2020d). Differences in mobility and bioavailability of these fractions has attracted much research interest, and isotope variation among different geochemical fractions of soil metals is an interesting phenomenon. In order to examine the isotope variation between labile and non-labile metal fractions, a combination of conventional sequential extraction methods and stable isotope analyses approaches have been adopted by several studies.

It has been noted that the isotope variation among geochemical fractions is affected by the contact time of the metal with the soil, termed aging. The aging of the stable isotope signal of metals has been confirmed by a spiking study (Huang et al. 2014), where ^{206}Pb was introduced as an exogenous Pb source through spiking for 30 days. After spiking, $^{208}Pb/^{206}Pb$ values decrease in labile forms (i.e. acid-extractable fractions in the BCR procedure), while the values remained stable in the residual fractions. This phenomenon confirmed that external sources of metals are more likely to affect labile fractions first. Another study by Shetaya et al. (2019) found that the influence of external inputs may affect other fractions gradually, thus diminishing the isotope variation effect in the long term. Shetaya et al. (2019) examined various geochemical fractions (i.e., exchangeable, bound to carbonates, bound to Fe-Mn oxides, bound to organic matter, residual) as well as the $^{206}Pb/^{207}Pb$, $^{208}Pb/^{207}Pb$ ratios in each fraction. No significant differences among isotope ratios were observed among the different phases, indicating that anthropogenic Pb sources did not possess preferential affinity

838 towards more labile forms than other forms. In this sense, anthropogenic Pb is
839 sufficiently labile to be assimilated into geochemical pools. This may be due to the
840 relatively long contact time enabled the redistribution of geochemical forms, but no
841 experimental studies have been undertaken to test this hypothesis to date. In
842 conclusion, isotope ratios of labile metal pools may reflect the influence of
843 anthropogenic sources, while those of less-labile pools reveal the lithogenic origins.
844 The aging of the isotope signals of externally introduced metals into soil might be useful
845 for distinguishing recent from historical contamination. Distinct variations amongst
846 geochemical fractionations would indicate recent contamination, while no variations
847 would indicate historical contamination.
848

849 # 6 Challenges and outlook

850 Stable isotope analysis can provide information on metal sources and has been
851 successfully applied for quantitative or qualitative source identification purposes.
852 However, several challenges remain in this field:
853 1) Analytical challenges hinder the application of metal stable isotope analysis
854 approaches. High-quality pretreatment, such as ion-exchange, is the prerequisite
855 for the accurate and precise determination of metal isotopes. High-precision
856 analysis approaches (by MC-ICP-MS or TIMS) are time-consuming and costly,
857 rendering them unsuitable for large numbers of samples. Future studies should
858 seek for more efficient sample purification strategies, and explore the feasibility of

conventional ICP-QMS for the rapid “fit-for-purpose” determination of metal isotopes with proper mass bias correction methods.

2) The selection of the environmental samples for source apportionment should be conducted with care. If the investigated area is large, collecting only a few environmental samples (e.g., fly ash, slag, road dust, fertilizer, soil) may bias the source apportionment because the natural heterogeneity of these materials is not sufficiently covered. Several studies have adopted available isotopic data from literature, even if the soil characteristics, lithology, major anthropogenic emission sources and dominating fractionation mechanisms are quite different. This should be avoided, since large intra-material variations in stable isotope ratios have been observed for metals (Figures 1-5). Extrapolating reference ratios from the literature to a specific source apportionment case study may result in misinterpretation of isotope data. Instead, before collecting environmental samples, a pre-understanding of potential pollution sources is required. For instance, if the soil is in the vicinity of an industrial facility (e.g., coal-fired power plant, metal smelter), it is necessary to collect detailed information about potential contamination pathways (e.g., through atmospheric deposition of fine particles or via waste leaching) in advance. For a contaminated agricultural field, knowledge of the used fertilizer and pesticide types as well as potential irrigation sources will be necessary for the collection of representative samples.

3) Isotope fractionation mechanisms are still poorly understood. For most metals

(e.g., Cu, Zn, Cd, Hg, Tl), isotopic variations are induced by fractionating processes. Geochemical processes in soils, such as adsorption, dissolution, redox reactions and biological processes can result in substantial isotope fractionations, thus blurring the source signals. To avoid misinterpretation of isotopic data, a comprehensive and in-depth understanding of the fractionation processes is therefore required. But even if the latter can be reached, the complexity of isotope-fractionating processes can impede source identification.

4) The use of a single isotope ratio may fail in source apportionment, because the variation of the considered isotope ratio can vary more strongly within a source than between different sources. Furthermore, different sources may share similar isotopic compositions (Section 3.4), making multi-source identification impossible. To overcome these obstacles, one can conduct source apportionment in a two-dimensional space, that is, to use another isotope (either from the same element or another) when isotope signatures overlapped. For instance, a combination of Sr and Pb isotopes has been successfully applied for source apportionment (Section 3.4). Analyzing the isotopic ratios on the 2-D MIF-MDF plot of Hg clearly reveals the influence of diverse sources, even if Hg-MDF signatures often overlap (Figure 4).

Successful attempts of stable isotope-based pollution source identification in other environmental media can shed light on soil metal source apportionment. For instance, the distinct MIF fractionation in Hg analysis has been widely used for air pollution

source tracking (Fu et al. 2019; Kurz et al. 2020). Considering that long-range transport could be a significant source of soil metals (especially for Hg), these stable isotope variations could serve as valuable references for future studies.

Undoubtedly, investigations on metal stable isotopes are moving at a fast pace. Our understanding of these non-traditional isotopes for the source identification of metals in soil is still incomplete, and many questions remain open.

Acknowledgements

This work was supported by the the National Natural Science Foundation of China (Grant No. 42077118), and National Key Research and Development Program of China (Grant No. 2020YFC1808000). Nina J. Schleicher acknowledges the German Research Foundation (DFG) for financial support (SCHL 1908/2-1).

References

Aebischer, S.; Cloquet, C.; Carignan, J.; Maurice, C.; Pienitz, R. Disruption of the geochemical metal cycle during mining: Multiple isotope studies of lake sediments from Schefferville, subarctic Québec. Chem. Geol. 2015;412:167-178

Alloway, B.J. Heavy metals in soils: trace metals and metalloids in soils and their bioavailability. Springer Science & Business Media; 2012

Alloway, B.J. Heavy Metals in Soils Trace Metals and Metalloids in Soils and their Bioavailability.3rd ed.. Dordrecht : Springer Netherlands : Imprint: Springer; 2013

Araújo, D.F.; Boaventura, G.R.; Machado, W.; Viers, J.; Weiss, D.; Patchineelam, S.R.; Ruiz, I.; Rodrigues, A.P.C.; Babinski, M.; Dantas, E. Tracing of anthropogenic zinc sources in coastal environments using stable isotope composition. Chem. Geol. 2017;449:226-235

Araújo, D.F.; Machado, W.; Weiss, D.; Mulholland, D.S.; Garnier, J.; Souto-Oliveira, C.E.; Babinski, M. Zinc isotopes as tracers of anthropogenic sources and biogeochemical processes in contaminated mangroves. Appl. Geochem. 2018;95:25-32

Araújo, D.F.; Ponzevera, E.; Briant, N.; Knoery, J.; Sireau, T.; Mojtahid, M.; Metzger, E.; Brach-Papa, C. Assessment of the metal contamination evolution in the Loire estuary using Cu and Zn stable isotopes and geochemical data in sediments. Mar. Pollut. Bull. 2019;143:12-23

Atafar, Z.; Mesdaghinia, A.; Nouri, J.; Homaee, M.; Yunesian, M.; Ahmadimoghaddam, M.; Mahvi, A.H. Effect of fertilizer application on soil heavy metal concentration. Environ. Monit. Assess. 2010;160:83-89

Ayuso, R.A.; Foley, N.K. Lead and Strontium Isotopes as Monitors of Anthropogenic Contaminants in the Surficial Environment. Environmental Geochemistry: Site Characterization, Data Analysis and Case Histories: Second Edition; 2018

Babcsanyi, I.; Chabaux, F.; Granet, M.; Meite, F.; Payraudeau, S.; Duplay, J.; Imfeld, G. Copper in soil fractions and runoff in a vineyard catchment: Insights from copper stable isotopes. Sci. Total Environ. 2016;557:154-162

Baptista-Salazar, C.; Hintelmann, H.; Biester, H. Distribution of mercury species and mercury isotope ratios in soils and river suspended matter of a mercury mining area. Environ. Sci. Process. Impacts 2018;20:621-631

Barraza, F.; Moore, R.E.T.; Rehkämper, M.; Schreck, E.; Lefeuvre, G.; Kreissig, K.; Coles, B.J.; Maurice, L. Cadmium isotope fractionation in the soil-cacao systems of Ecuador: A pilot field study. RSC Adv. 2019;9:34011-34022

Berna, E.C.; Johnson, T.M.; Makdisi, R.S.; Basu, A. Cr stable isotopes as indicators of Cr(VI) reduction in groundwater: A detailed time-series study of a point-source plume. Environ. Sci. Technol. 2010;44:1043-1048

Bigalke, M.; Kersten, M.; Weyer, S.; Wilcke, W. Isotopes trace biogeochemistry and sources of Cu and Zn in an intertidal soil wetland soils. Soil Sci. Soc. Am. J. 2013;77:680-691

Bigalke, M.; Weyer, S.; Kobza, J.; Wilcke, W. Stable Cu and Zn isotope ratios as tracers of sources and transport of Cu and Zn in contaminated soil. Geochim. Cosmochim. Acta 2010;74:6801-6813

Bigalke, M.; Weyer, S.; Wilcke, W. Stable Cu isotope fractionation in soils during oxic weathering and podzolization. Geochim. Cosmochim. Acta 2011;75:3119-3134

Bigeleisen, J. Nuclear size and shape effects in chemical reactions. Isotope chemistry of the heavy elements. J. AM. CHEM. SOC. 1996;118:3676-3680

Bińczycki, T.; Weber, J.; Mielnik, L.; Asensio, C. Lead isotope ratios in Podzol profiles as a tracer of pollution source in the subalpine zone of the Karkonosze National Park, Sudety Mts (south-western Poland). Catena 2020;189

Bing, H.; Wu, Y.; Zhou, J.; Ming, L.; Sun, S.; Li, X. Atmospheric deposition of lead in remote high mountain of eastern Tibetan Plateau, China. Atmos. Environ. 2014;99:425-435

Bio-Rad Laboratories. Instruction Manual, AG® 1, AG MP-1, and AG 2 Strong Anion Exchange Resin, Rev C. LIT212. 2020

Biswas, A.; Blum, J.D.; Bergquist, B.A.; Keeler, G.J.; Xie, Z. Natural mercury isotope variation in coal deposits and organic soils. Environ. Sci. Technol. 2008;42:8303-8309

Blotevogel, S.; Oliva, P.; Sobanska, S.; Viers, J.; Vezin, H.; Audry, S.; Prunier, J.; Darrozes, J.; Orgogozo, L.; Courjault-Radé, P.; Schreck, E. The fate of Cu pesticides in vineyard soils: A case study using δ65Cu isotope ratios and EPR analysis. Chem. Geol. 2018;477:35-46

Blum, J.D.; Johnson, M.W. Recent developments in mercury stable isotope analysis. Reviews in Mineralogy and Geochemistry; 2017

Blum, J.D.; Sherman, L.S.; Johnson, M.W. Mercury isotopes in earth and environmental sciences. Annual Review of Earth and Planetary Sciences; 2014

971 Borrok, D.M.; Gieré, R.; Ren, M.; Landa, E.R. Zinc isotopic composition of particulate matter generated
972 during the combustion of coal and coal + tire-derived fuels. Environ. Sci. Technol.
973 2010;44:9219-9224
974 Bryan, A.L.; Dong, S.; Wilkes, E.B.; Wasylenki, L.E. Zinc isotope fractionation during adsorption onto Mn
975 oxyhydroxide at low and high ionic strength. Geochim. Cosmochim. Acta 2015;157:182-197
976 Buchachenko, A.L. Magnetic isotope effect: Nuclear spin control of chemical reactions. J Phys Chem A
977 2001;105
978 Bullen, T.D. 7.10 - Metal Stable Isotopes in Weathering and Hydrology. in: Holland H.D., Turekian K.K.
979 Treatise on Geochemistry (Second Edition). Oxford: Elsevier; 2014
980 Čadková, E.; Chrastný, V. Isotope evidence of hexavalent chromium stability in ground water samples.
981 Chemosphere 2015;138:74-80
982 Cheema, A.I.; Liu, G.; Yousaf, B.; Abbas, Q.; Zhou, H. A comprehensive review of biogeochemical
983 distribution and fractionation of lead isotopes for source tracing in distinct interactive
984 environmental compartments. Sci. Total Environ. 2020:135658
985 Chen, H.; Teng, Y.; Lu, S.; Wang, Y.; Wang, J. Contamination features and health risk of soil heavy metals
986 in China. Sci. Total Environ. 2015;512-513:143-153
987 Chen, J.; Gaillardet, J.; Louvat, P. Zinc isotopes in the Seine River waters, France: A probe of
988 anthropogenic contamination. Environ. Sci. Technol. 2008;42:6494-6501
989 Chen, J.; Hintelmann, H.; Feng, X.; Dimock, B. Unusual fractionation of both odd and even mercury
990 isotopes in precipitation from Peterborough, ON, Canada. Geochim. Cosmochim. Acta
991 2012;90:33-46
992 Chen, L.; Zhou, S.; Wu, S.; Wang, C.; He, D. Concentration, fluxes, risks, and sources of heavy metals in
993 atmospheric deposition in the Lihe River watershed, Taihu region, eastern China. Environ.
994 Pollut. 2019;225
995 Chen, L.; Zhou, S.; Wu, S.; Wang, C.; Li, B.; Li, Y.; Wang, J. Combining emission inventory and isotope ratio
996 analyses for quantitative source apportionment of heavy metals in agricultural soil.
997 Chemosphere 2018;204:140-147
998 Cheng, H.F.; Hu, Y.A. Lead (Pb) isotopic fingerprinting and its applications in lead pollution studies in
999 China: A review. Environ. Pollut. 2010;158:1134-1146
1000 Chrastný, V.; Čadková, E.; Vaněk, A.; Teper, L.; Cabala, J.; Komárek, M. Cadmium isotope fractionation
1001 within the soil profile complicates source identification in relation to Pb-Zn mining and smelting
1002 processes. Chem. Geol. 2015;405:1-9
1003 Cloquet, C.; Carignan, J.; Libourel, G. Isotopic composition of Zn and Pb atmospheric depositions in an
1004 urban/periurban area of northeastern France. Environ. Sci. Technol. 2006a;40:6594-6600
1005 Cloquet, C.; Carignan, J.; Libourel, G.; Sterckeman, T.; Perdrix, E. Tracing source pollution in soils using
1006 cadmium and lead isotopes. Environ. Sci. Technol. 2006b;40:2525-2530
1007 Craig, H. Standard for Reporting Concentrations of Deuterium and Oxygen-18 in Natural Waters. Science
1008 1961;133:1833-&
1009 Cui, B.; Zhu, M.; Jiang, Y.; Jiang, Y.; Cao, H. Identification of the sources of metals and arsenic in river
1010 sediments by multivariate analysis and geochemical approaches. J. Soils Sed. 2014;14:1456-
1011 1468
1012 Dawson, J.J.C.; Tetzlaff, D.; Carey, A.M.; Raab, A.; Soulsby, C.; Killham, K.; Meharg, A.A. Characterizing Pb

Mobilization from Upland Soils to Streams Using Pb-206/Pb-207 Isotopic Ratios. Environ. Sci. Technol. 2010;44:243-249

De Silva, S.; Ball, A.S.; Huynh, T.; Reichman, S.M. Metal accumulation in roadside soil in Melbourne, Australia: Effect of road age, traffic density and vehicular speed. Environ. Pollut. 2016;208:102-109

Delattre, E.; Techer, I.; Reneaud, B.; Thireau, V.; Verdoux, P.; Prohin, P. Sr isotope discrimination of multi species aquaculture productions at a worldwide scale and contribution of the water reservoir in Sr plant input. Heliyon 2020;6

Deng, J.; Wang, C.; Bagas, L.; Selvaraja, V.; Jeon, H.; Wu, B.; Yang, L. Insights into ore genesis of the Jinding Zn–Pb deposit, Yunnan Province, China: Evidence from Zn and in-situ S isotopes. Ore Geol. Rev. 2017;90:943-957

Desaulty, A.M.; Petelet-Giraud, E. Zinc isotope composition as a tool for tracing sources and fate of metal contaminants in rivers. Sci. Total Environ. 2020;728

Dolgopolova, A.; Weiss, D.J.; Seltmann, R.; Kober, B.; Mason, T.F.D.; Coles, B.; Stanley, C.J. Use of isotope ratios to assess sources of Pb and Zn dispersed in the environment during mining and ore processing within the Orlovka-Spokoinoe mining site (Russia). Appl. Geochem. 2006;21:563-579

Dong, S.; Ochoa Gonzalez, R.; Harrison, R.M.; Green, D.; North, R.; Fowler, G.; Weiss, D. Isotopic signatures suggest important contributions from recycled gasoline, road dust and non-exhaust traffic sources for copper, zinc and lead in PM10 in London, United Kingdom. Atmos. Environ. 2017;165:88-98

Dótor-Almazán, A.; Armienta-Hernández, M.A.; Talavera-Mendoza, O.; Ruiz, J. Geochemical behavior of Cu and sulfur isotopes in the tropical mining region of Taxco, Guerrero (southern Mexico). Chem. Geol. 2017;471:1-12

Driscoll, C.T.; Mason, R.P.; Chan, H.M.; Jacob, D.J.; Pirrone, N. Mercury as a global pollutant: Sources, pathways, and effects. Environ. Sci. Technol. 2013;47:4967-4983

Du, Z.; Xiao, C.; Liu, Y.; Yang, J.; Li, C. Natural vs. anthropogenic sources supply aeolian dust to the Miaoergou Glacier: Evidence from Sr–Pb isotopes in the eastern Tienshan ice core. Quat. Int. 2017;430:60-70

Ellis, A.S.; Johnson, T.M.; Bullen, T.D. Chromium isotopes and the fate of hexavalent chromium in the environment. Science 2002;295:2060-2062

Erel, Y.; Torrent, J. Contribution of Saharan dust to Mediterranean soils assessed by sequential extraction and Pb and Sr isotopes. Chem. Geol. 2010;275:19-25

Estrade, N.; Carignan, J.; Donard, O.F.X. Tracing and quantifying anthropogenic mercury sources in soils of northern France using isotopic signatures. Environ. Sci. Technol. 2011;45:1235-1242

Fekiacova, Z.; Cornu, S.; Pichat, S. Tracing contamination sources in soils with Cu and Zn isotopic ratios. Sci. Total Environ. 2015;517:96-105

Feng, X.; Foucher, D.; Hintelmann, H.; Yan, H.; He, T.; Qiu, G. Tracing mercury contamination sources in sediments using mercury isotope compositions. Environ. Sci. Technol. 2010;44:3363-3368

Feng, X.B.; Yin, R.S.; Yu, B.; Du, B.Y. Mercury isotope variations in surface soils in different contaminated areas in Guizhou Province, China. Chin. Sci. Bull. 2013;58:249-255

Fouskas, F.; Ma, L.; Engle, M.A.; Ruppert, L.; Geboy, N.J.; Costa, M.A. Cadmium isotope fractionation

during coal combustion: Insights from two US coal-fired power plants. Appl. Geochem. 2018;96:100-112

Fu, X.; Zhang, H.; Liu, C.; Zhang, H.; Lin, C.J.; Feng, X. Significant Seasonal Variations in Isotopic Composition of Atmospheric Total Gaseous Mercury at Forest Sites in China Caused by Vegetation and Mercury Sources. Environ. Sci. Technol. 2019;53:13748-13756

Gao, B.; Zhou, H.; Liang, X.; Tu, X. Cd isotopes as a potential source tracer of metal pollution in river sediments. Environ. Pollut. 2013;181:340-343

Geagea, M.L.; Stille, P.; Gauthier-Lafaye, F.; Millet, M. Tracing of industrial aerosol sources in an urban environment using Pb, Sr, and Nd isotopes. Environ. Sci. Technol. 2008;42:692-698

Ghosh, S.; Schauble, E.A.; Lacrampe Couloume, G.; Blum, J.D.; Bergquist, B.A. Estimation of nuclear volume dependent fractionation of mercury isotopes in equilibrium liquid-vapor evaporation experiments. Chem. Geol. 2013;336:5-12

Goix, S.; Maurice, L.; Laffont, L.; Rinaldo, R.; Lagane, C.; Chmeleff, J.; Menges, J.; Heimbürger, L.E.; Maury-Brachet, R.; Sonke, J.E. Quantifying the impacts of artisanal gold mining on a tropical river system using mercury isotopes. Chemosphere 2019;219:684-694

Gong, Y.; Qu, Y.; Yang, S.; Tao, S.; Shi, T.; Liu, Q.; Chen, Y.; Wu, Y.; Ma, J. Status of arsenic accumulation in agricultural soils across China (1985–2016). Environ. Res. 2020;186

Gonzalez, R.O.; Weiss, D. Zinc Isotope Variability in Three Coal-Fired Power Plants: A Predictive Model for Determining Isotopic Fractionation during Combustion. Environ. Sci. Technol. 2015;49:12560-12567

Gou, W.; Li, W.; Ji, J.; Li, W. Zinc Isotope Fractionation during Sorption onto Al Oxides: Atomic Level Understanding from EXAFS. Environ. Sci. Technol. 2018;52:9087-9096

Gratz, L.E.; Keeler, G.J.; Blum, J.D.; Sherman, L.S. Isotopic composition and fractionation of mercury in Great Lakes precipitation and ambient air. Environ. Sci. Technol. 2010;44:7764-7770

Gray, J.E.; Pribil, M.J.; Higueras, P.L. Mercury isotope fractionation during ore retorting in the Almadén mining district, Spain. Chem. Geol. 2013;357:150-157

Grösslová, Z.; Vaněk, A.; Oborná, V.; Mihaljevič, M.; Ettler, V.; Trubač, J.; Drahota, P.; Penížek, V.; Pavlů, L.; Sracek, O.; Kříbek, B.; Voegelin, A.; Göttlicher, J.; Drábek, O.; Tejnecký, V.; Houška, J.; Mapani, B.; Zádorová, T. Thallium contamination of desert soil in Namibia: Chemical, mineralogical and isotopic insights. Environ. Pollut. 2018;239:272-280

Heikoop, J.M.; Johnson, T.M.; Birdsell, K.H.; Longmire, P.; Hickmott, D.D.; Jacobs, E.P.; Broxton, D.E.; Katzman, D.; Vesselinov, V.V.; Ding, M.; Vaniman, D.T.; Reneau, S.L.; Goering, T.J.; Glessner, J.; Basu, A. Isotopic evidence for reduction of anthropogenic hexavalent chromium in Los Alamos National Laboratory groundwater. Chem. Geol. 2014;373:1-9

Hirata, T. Lead isotopic analyses of NIST standard reference materials using multiple collector inductively coupled plasma mass spectrometry coupled with a modified external correction method for mass discrimination effect. Analyst 1996;121:1407-1411

Hoefs, J. Stable Isotope Geochemistry, Eighth Edition. Berlin, Heidelberg : Springer Berlin Heidelberg : Imprint: Springer; 2018

Hosono, T.; Nakano, T.; Igeta, A.; Tayasu, I.; Tanaka, T.; Yachi, S. Impact of fertilizer on a small watershed of Lake Biwa: Use of sulfur and strontium isotopes in environmental diagnosis. Sci. Total Environ. 2007;384:342-354

1097 Hou, D. Sustainable Remediation of Contaminated Soil and Groundwater: Materials, Processes, and
1098 Assessment. Elsevier Inc.; 2020
1099 Hou, D.; O'Connor, D.; Igalavithana, A.D.; Alessi, D.S.; Luo, J.; Tsang, D.C.W.; Sparks, D.L.; Yamauchi, Y.;
1100 Rinklebe, J.; Ok, Y.S. Metal contamination and bioremediation of agricultural soils for food
1101 safety and sustainability. Nat. Rev. Earth Environ. 2020a;1:366-381
1102 Hou, R.; Wang, L.; O'Connor, D.; Tsang, D.C.; Rinklebe, J.; Hou, D. Effect of immobilizing reagents on soil
1103 Cd and Pb lability under freeze-thaw cycles: Implications for sustainable agricultural
1104 management in seasonally frozen land. Environment International 2020b;144:106040
1105 Huang, S.; Yuan, D.; Lin, H.; Sun, L.; Lin, S. Fractionation of mercury stable isotopes during coal
1106 combustion and seawater flue gas desulfurization. Appl. Geochem. 2017;76:159-167
1107 Huang, Y.; Zhang, S.; Chen, Y.; Wang, L.; Long, Z.; Hughes, S.S.; Ni, S.; Cheng, X.; Wang, J.; Li, T.; Wang, R.;
1108 Liu, C. Tracing Pb and Possible Correlated Cd Contamination in Soils by Using Lead Isotopic
1109 Compositions. J. Hazard. Mater. 2020;385
1110 Huang, Z.Y.; Xie, H.; Cao, Y.L.; Cai, C.; Zhang, Z. Assessing of distribution, mobility and bioavailability of
1111 exogenous Pb in agricultural soils using isotopic labeling method coupled with BCR approach.
1112 J. Hazard. Mater. 2014;266:182-188
1113 Hurst, R.W.; Davis, T.E. Strontium isotopes as tracers of airborne fly ash from coal-fired power plants.
1114 Environ. Geol. 1981;3:363-367
1115 Hurst, R.W.; Davis, T.E.; Elseewi, A.A. Strontium isotopes as tracers of coal combustion residue in the
1116 environment. Eng. Geol. 1991;30:59-77
1117 Imseng, M.; Wiggenhauser, M.; Keller, A.; Muller, M.; Rehkamper, M.; Murphy, K.; Kreissig, K.; Frossard,
1118 E.; Wilcke, W.; Bigalke, M. Fate of Cd in Agricultural Soils: A Stable Isotope Approach to
1119 Anthropogenic Impact, Soil Formation, and Soil-Plant Cycling. Environ. Sci. Technol.
1120 2018;52:1919-1928
1121 Imseng, M.; Wiggenhauser, M.; Keller, A.; Müller, M.; Rehkämper, M.; Murphy, K.; Kreissig, K.; Frossard,
1122 E.; Wilcke, W.; Bigalke, M. Towards an understanding of the Cd isotope fractionation during
1123 transfer from the soil to the cereal grain. Environ. Pollut. 2019a;244:834-844
1124 Imseng, M.; Wiggenhauser, M.; Müller, M.; Keller, A.; Frossard, E.; Wilcke, W.; Bigalke, M. The Fate of Zn
1125 in Agricultural Soils: A Stable Isotope Approach to Anthropogenic Impact, Soil Formation, and
1126 Soil-Plant Cycling. Environ. Sci. Technol. 2019b;53:4140-4149
1127 Irrgeher, J.; Prohaska, T. Application of non-traditional stable isotopes in analytical ecogeochemistry
1128 assessed by MC ICP-MS - A critical review. Anal. Bioanal. Chem. 2016;408:369-385
1129 Jamieson-Hanes, J.H.; Gibson, B.D.; Lindsay, M.B.J.; Kim, Y.; Ptacek, C.J.; Blowes, D.W. Chromium isotope
1130 fractionation during reduction of Cr(VI) under saturated flow conditions. Environ. Sci. Technol.
1131 2012;46:6783-6789
1132 Jeon, S.K.; Kwon, M.J.; Yang, J.S.; Lee, S. Identifying the source of Zn in soils around a Zn smelter using
1133 Pb isotope ratios and mineralogical analysis. Sci. Total Environ. 2017;601-602:66-72
1134 Jia, Z.; Wang, J.; Zhou, X.; Zhou, Y.; Li, Y.; Li, B.; Zhou, S. Identification of the sources and influencing
1135 factors of potentially toxic elements accumulation in the soil from a typical karst region in
1136 Guangxi, Southwest China. Environ. Pollut. 2020a;256
1137 Jia, Z.Y.; Wang, J.X.; Zhou, X.D.; Zhou, Y.J.; Li, Y.; Li, B.J.; Zhou, S.L. Identification of the sources and
1138 influencing factors of potentially toxic elements accumulation in the soil from a typical karst

region in Guangxi, Southwest China. Environ. Pollut. 2020b;256:9
Jiang, S.Z.; Luo, J.; Ye, Y.Q.; Yang, G.; Pi, W.; He, W.X. Using Pb Isotope to Quantify the Effect of Various Sources on Multi-Metal Polluted soil in Guiyu. Bull. Environ. Contam. Toxicol. 2019;102:413-418
Jiménez-Moreno, M.; Barre, J.P.G.; Perrot, V.; Bérail, S.; Rodríguez Martín-Doimeadios, R.C.; Amouroux, D. Sources and fate of mercury pollution in Almadén mining district (Spain): Evidences from mercury isotopic compositions in sediments and lichens. Chemosphere 2016;147:430-438
Jiménez-Moreno, M.; Perrot, V.; Epov, V.N.; Monperrus, M.; Amouroux, D. Chemical kinetic isotope fractionation of mercury during abiotic methylation of Hg(II) by methylcobalamin in aqueous chloride media. Chem. Geol. 2013;336:26-36
Jing, F.; Chen, X.M.; Wen, X.; Liu, W.; Hu, S.M.; Yang, Z.J.; Guo, B.L.; Luo, Y.; Yu, Q.X.; Xu, Y.L. Biochar effects on soil chemical properties and mobilization of cadmium (Cd) and lead (Pb) in paddy soil. Soil Use Manage. 2019:8
Jiskra, M.; Wiederhold, J.G.; Bourdon, B.; Kretzschmar, R. Solution speciation controls mercury isotope fractionation of Hg(II) sorption to goethite. Environ. Sci. Technol. 2012;46:6654-6662
Jiskra, M.; Wiederhold, J.G.; Skyllberg, U.; Kronberg, R.M.; Kretzschmar, R. Source tracing of natural organic matter bound mercury in boreal forest runoff with mercury stable isotopes. Environ. Sci. Process. Impacts 2017;19:1235-1248
Jonhson, T.M.; Bullen, T.D. Mass-dependent fractionation of selenium and chromium isotopes in low-temperature environments. Reviews in Mineralogy and Geochemistry; 2004
Jouvin, D.; Weiss, D.J.; Mason, T.F.M.; Bravin, M.N.; Louvat, P.; Zhao, F.; Ferec, F.; Hinsinger, P.; Benedetti, M.F. Stable isotopes of Cu and Zn in higher plants: Evidence for Cu reduction at the root surface and two conceptual models for isotopic fractionation processes. Environ. Sci. Technol. 2012;46:2652-2660
Kang, M.J.; Kwon, Y.K.; Yu, S.; Lee, P.K.; Park, H.S.; Song, N. Assessment of Zn pollution sources and apportionment in agricultural soils impacted by a Zn smelter in South Korea. J. Hazard. Mater. 2019;364:475-487
Kazakis, N.; Kantiranis, N.; Kalaitzidou, K.; Kaprara, M.; Mitrakas, M.; Frei, R.; Vargemezis, G.; Tsourlos, P.; Zouboulis, A.; Filippidis, A. Origin of hexavalent chromium in groundwater: The example of Sarigkiol Basin, Northern Greece. Sci. Total Environ. 2017;593-594:552-566
Kelepertzis, E.; Argyraki, A.; Chrastný, V.; Botsou, F.; Skordas, K.; Komárek, M.; Fouskas, A. Metal(loid) and isotopic tracing of Pb in soils, road and house dusts from the industrial area of Volos (central Greece). Sci. Total Environ. 2020;725
Kelepertzis, E.; Komarek, M.; Argyraki, A.; Sillerova, H. Metal(loid) distribution and Pb isotopic signatures in the urban environment of Athens, Greece. Environ. Pollut. 2016;213:420-431
Kersten, M.; Xiao, T.; Kreissig, K.; Brett, A.; Coles, B.J.; Rehkämper, M. Tracing anthropogenic thallium in soil using stable isotope compositions. Environ. Sci. Technol. 2014;48:9030-9036
Kim, D.M.; Oh, Y.S.; Lee, J.S. δ34S and δ18O of sulfates and Zn/Cd ratios reveal the cause of soil and groundwater contamination in metalliferous mining areas. J. Geochem. Explor. 2020;209
Komarek, M.; Ettler, V.; Chrastny, V.; Mihaljevic, M. Lead isotopes in environmental sciences: A review. Environ. Int. 2008;34:562-577
Kong, H.; Teng, Y.; Song, L.; Wang, J.; Zhang, L. Lead and strontium isotopes as tracers to investigate the

potential sources of lead in soil and groundwater: A case study of the Hun River alluvial fan. Appl. Geochem. 2018;97:291-300

Kribek, B.; Sipkova, A.; Ettler, V.; Mihaljevic, M.; Majer, V.; Knesl, I.; Mapani, B.; Penizek, V.; Vanek, A.; Sracek, O. Variability of the copper isotopic composition in soil and grass affected by mining and smelting in Tsumeb, Namibia. Chem. Geol. 2018;493:121-135

Kříbek, B.; Zachariáš, J.; Knésl, I.; Míková, J.; Mihaljevič, M.; Veselovský, F.; Bamba, O. Geochemistry, mineralogy, and isotope composition of Pb, Zn, and Cu in primary ores, gossan and barren ferruginous crust from the Perkoa base metal deposit, Burkina Faso. J. Geochem. Explor. 2016;168:49-64

Kume, T.; Akca, E.; Nakano, T.; Nagano, T.; Kapur, S.; Watanabe, T. Seasonal changes of fertilizer impacts on agricultural drainage in a salinized area in Adana, Turkey. Sci. Total Environ. 2010;408:3319-3326

Kurz, A.Y.; Blum, J.D.; Gratz, L.E.; Jaffe, D.A. Contrasting Controls on the Diel Isotopic Variation of Hg0at Two High Elevation Sites in the Western United States. Environ. Sci. Technol. 2020;54:10502-10513

Kusonwiriyawong, C.; Bigalke, M.; Abgottspon, F.; Lazarov, M.; Wilcke, W. Response of Cu partitioning to flooding: A δ65Cu approach in a carbonatic alluvial soil. Chem. Geol. 2016;420:69-76

Lee, P.-K.; Kang, M.-J.; Jeong, Y.-J.; Kwon, Y.K.; Yu, S. Lead isotopes combined with geochemical and mineralogical analyses for source identification of arsenic in agricultural soils surrounding a zinc smelter. J. Hazard. Mater. 2020a;382:121044-121044

Lee, P.K.; Kang, M.J.; Yu, S.; Kwon, Y.K. Assessment of trace metal pollution in roof dusts and soils near a large Zn smelter. Sci. Total Environ. 2020b;713

Li, D.D.; Liu, S.A.; Li, S.G. Copper isotope fractionation during adsorption onto kaolinite: Experimental approach and applications. Chem. Geol. 2015;396:74-82

Li, H.B.; Yu, S.; Li, G.L.; Deng, H.; Luo, X.S. Contamination and source differentiation of Pb in park soils along an urban-rural gradient in Shanghai. Environ. Pollut. 2011;159:3536-3544

Li, J.; Zhang, G.; Ruan, L.; Yang, J.; Wang, H. Sr-Nd elements and isotopes as tracers of dust input in a tropical soil chronosequence. Geoderma 2016;262:227-234

Li, W.; Gou, W.X.; Li, W.Q.; Zhang, T.Y.; Yu, B.; Liu, Q.; Shi, J.B. Environmental applications of metal stable isotopes: Silver, mercury and zinc. Environ. Pollut. 2019;252:1344-1356

Lin, C.; Yu, R.; Hu, G.; Yang, Q.; Wang, X. Contamination and isotopic composition of Pb and Sr in offshore surface sediments from Jiulong River, Southeast China. Environ. Pollut. 2016;218:644-650

Liu, G.; Tao, L.; Liu, X.; Hou, J.; Wang, A.; Li, R. Heavy metal speciation and pollution of agricultural soils along Jishui River in non-ferrous metal mine area in Jiangxi Province, China. J. Geochem. Explor. 2013;132:156-163

Liu, J.; Wang, D.; Song, B.; Chen, Z.; Zhang, X.; Tang, Y. Source apportionment of Pb in a rice-soil system using field monitoring and isotope composition analysis. J. Geochem. Explor. 2019a;204:83-89

Liu, J.; Wang, J.; Chen, Y.; Shen, C.C.; Jiang, X.; Xie, X.; Chen, D.; Lippold, H.; Wang, C. Thallium dispersal and contamination in surface sediments from South China and its source identification. Environ. Pollut. 2016;213:878-887

Liu, J.; Wei, X.; Zhou, Y.; Tsang, D.C.W.; Bao, Z.; Yin, M.; Lippold, H.; Yuan, W.; Wang, J.; Feng, Y.; Chen, D. Thallium contamination, health risk assessment and source apportionment in common

vegetables. Sci. Total Environ. 2019b;

Liu, J.; Wei, X.; Zhou, Y.; Tsang, D.C.W.; Bao, Z.; Yin, M.; Lippold, H.; Yuan, W.; Wang, J.; Feng, Y.; Chen, D. Thallium contamination, health risk assessment and source apportionment in common vegetables. Sci. Total Environ. 2020a;703

Liu, J.; Yin, M.; Xiao, T.; Zhang, C.; Tsang, D.C.W.; Bao, Z.; Zhou, Y.; Chen, Y.; Luo, X.; Yuan, W.; Wang, J. Thallium isotopic fractionation in industrial process of pyrite smelting and environmental implications. J. Hazard. Mater. 2020b;384

Liu, S.A.; Teng, F.Z.; Li, S.; Wei, G.J.; Ma, J.L.; Li, D. Copper and iron isotope fractionation during weathering and pedogenesis: Insights from saprolite profiles. Geochim. Cosmochim. Acta 2014;146:59-75

Liu, T.; Zhu, C.; Yang, G.; Zhang, G.; Fan, H.; Zhang, Y.; Wen, H. Primary study of germanium isotope composition in sphalerite from the Fule Pb–Zn deposit, Yunnan province. Ore Geol. Rev. 2020c;120

Luo, X.S.; Xue, Y.; Wang, Y.L.; Cang, L.; Xu, B.; Ding, J. Source identification and apportionment of heavy metals in urban soil profiles. Chemosphere 2015;127:152-157

Luo, X.S.; Yu, S.; Zhu, Y.G.; Li, X.D. Trace metal contamination in urban soils of China. Sci. Total Environ. 2012;421-422:17-30

Luo, Y.; Teng, Y. Regional Difference in Soil Pollution and Strategy of Soil Zonal Governance and Remediation in China. Bulletin of the Chinese Academy of Sciences 2018;33:145-152

Lv, Y.; Liu, S.A.; Teng, F.Z.; Wei, G.J.; Ma, J.L. Contrasting zinc isotopic fractionation in two mafic-rock weathering profiles induced by adsorption onto Fe (hydr)oxides. Chem. Geol. 2020;539

Lv, Y.; Liu, S.A.; Zhu, J.M.; Li, S. Copper and zinc isotope fractionation during deposition and weathering of highly metalliferous black shales in central China. Chem. Geol. 2016;445:24-35

Malan, M.; Müller, F.; Cyster, L.; Raitt, L.; Aalbers, J. Heavy metals in the irrigation water, soils and vegetables in the Philippi horticultural area in the Western Cape Province of South Africa. Environ. Monit. Assess. 2015;187:1-8

Maréchal, C.N.; Télouk, P.; Albarède, F. Precise analysis of copper and zinc isotopic compositions by plasma-source mass spectrometry. Chem. Geol. 1999;156:251-273

Markl, G.; Lahaye, Y.; Schwinn, G. Copper isotopes as monitors of redox processes in hydrothermal mineralization. Geochim. Cosmochim. Acta 2006;70:4215-4228

Marković, T.; Manzoor, S.; Humphreys-Williams, E.; Kirk, G.J.D.; Vilar, R.; Weiss, D.J. Experimental Determination of Zinc Isotope Fractionation in Complexes with the Phytosiderophore 2′-Deoxymugeneic Acid (DMA) and Its Structural Analogues, and Implications for Plant Uptake Mechanisms. Environ. Sci. Technol. 2017;51:98-107

Martin, A.; Caldelas, C.; Weiss, D.; Aranjuelo, I.; Navarro, E. Assessment of Metal Immission in Urban Environments Using Elemental Concentrations and Zinc Isotope Signatures in Leaves of Nerium oleander. Environ. Sci. Technol. 2018;52:2071-2080

Martinková, E.; Chrastný, V.; Francová, M.; Šípková, A.; Čuřík, J.; Myška, O.; Mižič, L. Cadmium isotope fractionation of materials derived from various industrial processes. J. Hazard. Mater. 2016;302:114-119

Mason, T.F.D.; Weiss, D.J.; Chapman, J.B.; Wilkinson, J.J.; Tessalina, S.G.; Spiro, B.; Horstwood, M.S.A.; Spratt, J.; Coles, B.J. Zn and Cu isotopic variability in the Alexandrinka volcanic-hosted massive

sulphide (VHMS) ore deposit, Urals, Russia. Chem. Geol. 2005;221:170-187

Mathur, R.; Jin, L.; Prush, V.; Paul, J.; Ebersole, C.; Fornadel, A.; Williams, J.Z.; Brantley, S. Cu isotopes and concentrations during weathering of black shale of the Marcellus Formation, Huntingdon County, Pennsylvania (USA). Chem. Geol. 2012;304-305:175-184

Matt, P.; Powell, W.; Mathur, R.; deLorraine, W.F. Zn-isotopic evidence for fluid-assisted ore remobilization at the Balmat Zinc Mine, NY. Ore Geol. Rev. 2020;116

Mattielli, N.; Petit, J.C.J.; Deboudt, K.; Flament, P.; Perdrix, E.; Taillez, A.; Rimetz-Planchon, J.; Weis, D. Zn isotope study of atmospheric emissions and dry depositions within a 5 km radius of a Pb-Zn refinery. Atmos. Environ. 2009;43:1265-1272

Meier-Augenstein, W.; Schimmelmann, A. A guide for proper utilisation of stable isotope reference materials. Isot. Environ. Health Stud. 2019;55:113-128

Mihaljevic, M.; Baieta, R.; Ettler, V.; Vanek, A.; Kribek, B.; Penizek, V.; Drahota, P.; Trubac, J.; Sracek, O.; Chrastny, V.; Mapani, B.S. Tracing the metal dynamics in semi-arid soils near mine tailings using stable Cu and Pb isotopes. Chem. Geol. 2019;515:61-76

Moeller, K.; Schoenberg, R.; Pedersen, R.B.; Weiss, D.; Dong, S. Calibration of the New Certified Reference Materials ERM-AE633 and ERM-AE647 for Copper and IRMM-3702 for Zinc Isotope Amount Ratio Determinations. Geostandards Geoanalytical Res. 2012;36:177-199

Mondillo, N.; Wilkinson, J.J.; Boni, M.; Weiss, D.J.; Mathur, R. A global assessment of Zn isotope fractionation in secondary Zn minerals from sulfide and non-sulfide ore deposits and model for fractionation control. Chem. Geol. 2018;500:182-193

Morera-Gómez, Y.; Alonso-Hernández, C.M.; Santamaría, J.M.; Elustondo, D.; Lasheras, E.; Widory, D. Levels, spatial distribution, risk assessment, and sources of environmental contamination vectored by road dust in Cienfuegos (Cuba) revealed by chemical and C and N stable isotope compositions. Environ. Sci. Pollut. Res. 2020;27:2184-2196

Navarrete, J.U.; Borrok, D.M.; Viveros, M.; Ellzey, J.T. Copper isotope fractionation during surface adsorption and intracellular incorporation by bacteria. Geochim. Cosmochim. Acta 2011;75:784-799

O'Connor, D.; Hou, D.; Ok, Y.S.; Lanphear, B.P. The effects of iniquitous lead exposure on health. Nature Sustainability 2020;3:77-79

Pallavicini, N.; Engström, E.; Baxter, D.C.; Öhlander, B.; Ingri, J.; Rodushkin, I. Cadmium isotope ratio measurements in environmental matrices by MC-ICP-MS. J. Anal. At. Spectrom. 2014;29:1570-1584

Peng, M.; Zhao, C.; Ma, H.; Yang, Z.; Yang, K.; Liu, F.; Li, K.; Yang, Z.; Tang, S.; Guo, F.; Liu, X.; Cheng, H. Heavy metal and Pb isotopic compositions of soil and maize from a major agricultural area in Northeast China: Contamination assessment and source apportionment. J. Geochem. Explor. 2020;208

Petit, J.C.J.; Schäfer, J.; Coynel, A.; Blanc, G.; Deycard, V.N.; Derriennic, H.; Lanceleur, L.; Dutruch, L.; Bossy, C.; Mattielli, N. Anthropogenic sources and biogeochemical reactivity of particulate and dissolved Cu isotopes in the turbidity gradient of the Garonne River (France). Chem. Geol. 2013;359:125-135

Pribil, M.J.; Rimondi, V.; Costagliola, P.; Lattanzi, P.; Rutherford, D.L. Assessing mercury distribution using isotopic fractionation of mercury processes and sources adjacent and downstream of a legacy

mine district in Tuscany, Italy. Appl. Geochem. 2020;117
Qin, L.; Wang, X. Chromium isotope geochemistry. Reviews in Mineralogy and Geochemistry; 2017
Quevauviller, P.; Griepink, B.; Ure, A.; Muntaui, H. Improvement of analytical measurements within the bcr-programme: Single and sequential extraction procedures applied to soil and sediment analysis. Int. J. Environ. Anal. Chem. 1993;51:129-134
Raddatz, A.L.; Johnson, T.M.; McLing, T.L. Cr stable isotopes in snake river plain aquifer groundwater: Evidence for natural reduction of dissolved Cr(VI). Environ. Sci. Technol. 2011;45:502-507
Ruhl, L.S.; Dwyer, G.S.; Hsu-Kim, H.; Hower, J.C.; Vengosh, A. Boron and strontium isotopic characterization of coal combustion residuals: Validation of new environmental tracers. Environ. Sci. Technol. 2014;48:14790-14798
Rumble, J.R.; Lide, D.R.; Bruno, T.J. CRC handbook of chemistry and physics : a ready-reference book of chemical and physical data.99th edition. Boca Raton : CRC Press; 2018
Salmanzadeh, M.; Hartland, A.; Stirling, C.H.; Balks, M.R.; Schipper, L.A.; Joshi, C.; George, E. Isotope Tracing of Long-Term Cadmium Fluxes in an Agricultural Soil. Environ. Sci. Technol. 2017;51:7369-7377
Schoene, B. 4.10 - U–Th–Pb Geochronology. in: Holland H.D., Turekian K.K. Treatise on Geochemistry (Second Edition). Oxford: Elsevier; 2014
Schudel, G.; Kaplan, R.; Adler Miserendino, R.; Veiga, M.M.; Velasquez-López, P.C.; Guimarães, J.R.D.; Bergquist, B.A. Mercury isotopic signatures of tailings from artisanal and small-scale gold mining (ASGM) in southwestern Ecuador. Sci. Total Environ. 2019;686:301-310
Sherameti, I.; Varma, A. Heavy Metal Contamination of Soils Monitoring and Remediation.1st ed. 2015.. Cham : Springer International Publishing : Imprint: Springer; 2015
Sherman, L.S.; Blum, J.D.; Dvonch, J.T.; Gratz, L.E.; Landis, M.S. The use of Pb, Sr, and Hg isotopes in Great Lakes precipitation as a tool for pollution source attribution. Sci. Total Environ. 2015;502:362-374
Sherman, L.S.; Blum, J.D.; Johnson, K.P.; Keeler, G.J.; Barres, J.A.; Douglas, T.A. Mass-independent fractionation of mercury isotopes in Arctic snow driven by sunlight. Nat. Geosci. 2010;3:173-177
Sherman, L.S.; Blum, J.D.; Keeler, G.J.; Demers, J.D.; Dvonch, J.T. Investigation of local mercury deposition from a coal-fired power plant using mercury isotopes. Environ. Sci. Technol. 2012;46:382-390
Shetaya, W.H.; Marzouk, E.R.; Mohamed, E.F.; Bailey, E.H.; Young, S.D. Chemical and isotopic fractionation of lead in the surface soils of Egypt. Appl. Geochem. 2019;106:7-16
Shiel, A.E.; Weis, D.; Orians, K.J. Evaluation of zinc, cadmium and lead isotope fractionation during smelting and refining. Sci. Total Environ. 2010;408:2357-2368
Šillerová, H.; Chrastný, V.; Vítková, M.; Francová, A.; Jehlička, J.; Gutsch, M.R.; Kocourková, J.; Aspholm, P.E.; Nilsson, L.O.; Berglen, T.F.; Jensen, H.K.B.; Komárek, M. Stable isotope tracing of Ni and Cu pollution in North-East Norway: Potentials and drawbacks. Environ. Pollut. 2017;228:149-157
Sivry, Y.; Riotte, J.; Sonke, J.E.; Audry, S.; Schäfer, J.; Viers, J.; Blanc, G.; Freydier, R.; Dupré, B. Zn isotopes as tracers of anthropogenic pollution from Zn-ore smelters The Riou Mort-Lot River system. Chem. Geol. 2008;255:295-304
Smith, C.N.; Kesler, S.E.; Blum, J.D.; Rytuba, J.J. Isotope geochemistry of mercury in source rocks, mineral deposits and spring deposits of the California Coast Ranges, USA. Earth Plan. Sci. Lett.

2008;269:399-407
Stückrad, S.; Sabel, K.J.; Wilcke, W. Contributions of different parent materials in soils developed from periglacial cover-beds. Eur. J. Soil Sci. 2010;61:844-853
Sun, J.; Yu, R.; Hu, G.; Su, G.; Zhang, Y. Tracing of heavy metal sources and mobility in a soil depth profile via isotopic variation of Pb and Sr. Catena 2018;171:440-449
Sun, J.W.; Hu, G.R.; Yu, R.L.; Lin, C.Q.; Wang, X.M.; Huang, Y.Y. Human health risk assessment and source analysis of metals in soils along the G324 Roadside, China, by Pb and Sr isotopic tracing. Geoderma 2017;305:293-304
Sun, R. Mercury Stable Isotope Fractionation During Coal Combustion in Coal-Fired Boilers: Reconciling Atmospheric Hg Isotope Observations with Hg Isotope Fractionation Theory. Bull. Environ. Contam. Toxicol. 2019;102:657-664
Sun, R.; Sonke, J.E.; Heimbürger, L.E.; Belkin, H.E.; Liu, G.; Shome, D.; Cukrowska, E.; Liousse, C.; Pokrovsky, O.S.; Streets, D.G. Mercury stable isotope signatures of world coal deposits and historical coal combustion emissions. Environ. Sci. Technol. 2014a;48:7660-7668
Sun, R.; Sonke, J.E.; Liu, G.; Zheng, L.; Wu, D. Variations in the stable isotope composition of mercury in coal-bearing sequences: Indications for its provenance and geochemical processes. Int. J. Coal Geol. 2014b;133:13-23
Tan, S.C.; Zhou, J.X.; Li, B.; Zhao, J.X. In situ Pb and bulk Sr isotope analysis of the Yinchanggou Pb-Zn deposit in Sichuan Province (SW China): Constraints on the origin and evolution of hydrothermal fluids. Ore Geol. Rev. 2017;91:432-443
Tang, S.; Feng, C.; Feng, X.; Zhu, J.; Sun, R.; Fan, H.; Wang, L.; Li, R.; Mao, T.; Zhou, T. Stable isotope composition of mercury forms in flue gases from a typical coal-fired power plant, Inner Mongolia, northern China. J. Hazard. Mater. 2017;328:90-97
Tang, Y.T.; Cloquet, C.; Deng, T.H.B.; Sterckeman, T.; Echevarria, G.; Yang, W.J.; Morel, J.L.; Qiu, R.L. Zinc Isotope Fractionation in the Hyperaccumulator Noccaea caerulescens and the Nonaccumulating Plant Thlaspi arvense at Low and High Zn Supply. Environ. Sci. Technol. 2016;50:8020-8027
Techer, I.; Medini, S.; Janin, M.; Arregui, M. Impact of agricultural practice on the Sr isotopic composition of food products: Application to discriminate the geographic origin of olives and olive oil. Appl. Geochem. 2017;82:1-14
Tessier, A.; Campbell, P.G.C.; Bisson, M. SEQUENTIAL EXTRACTION PROCEDURE FOR THE SPECIATION OF PARTICULATE TRACE-METALS. Anal. Chem. 1979;51:844-851
Thomsen, E.; Andreasen, R. Agricultural lime disturbs natural strontium isotope variations: Implications for provenance and migration studies. Sci. Adv. 2019;5
Tomasevic, M.; Antanasijevic, D.; Anicic, M.; Deljanin, I.; Peric-Grujic, A.; Ristic, M. Lead concentrations and isotope ratios in urban tree leaves. Ecol. Indic. 2013;24:504-509
Tong, S.; Li, H.; Wang, L.; Tudi, M.; Yang, L. Concentration, Spatial Distribution, Contamination Degree and Human Health Risk Assessment of Heavy Metals in Urban Soils across China between 2003 and 2019-A Systematic Review. Int. J. Environ. Res. Public Health 2020;17
UN. Transforming our world: the 2030 Agenda for Sustainable Development. New York, USA: United Nations General Assembly; 2015
UNEP. Global Mercury Assessment. United Nations Environment Programme, Geneva 2018;

US EPA. Post-processing IsoSource Results. Retrieved from https://www.epa.gov/eco-research/post-processing-isosource-results. United States Environmental Protection Agency; 2016

US EPA. Stable Isotope Mixing Models for Estimating Source Proportions. Retrieved from https://www.epa.gov/eco-research/stable-isotope-mixing-models-estimating-source-proportions. United States Environmental Protection Agency; 2017

Vance, D.; Matthews, A.; Keech, A.; Archer, C.; Hudson, G.; Pett-Ridge, J.; Chadwick, O.A. The behaviour of Cu and Zn isotopes during soil development: Controls on the dissolved load of rivers. Chem. Geol. 2016;445:36-53

Vaněk, A.; Grösslová, Z.; Mihaljevič, M.; Ettler, V.; Trubač, J.; Chrastný, V.; Penížek, V.; Teper, L.; Cabala, J.; Voegelin, A.; Zádorová, T.; Oborná, V.; Drábek, O.; Holubík, O.; Houška, J.; Pavlů, L.; Ash, C. Thallium isotopes in metallurgical wastes/contaminated soils: A novel tool to trace metal source and behavior. J. Hazard. Mater. 2018;343:78-85

Vanek, A.; Grosslova, Z.; Mihaljevic, M.; Trubac, J.; Ettler, V.; Teper, L.; Cabala, J.; Rohovec, J.; Zadorova, T.; Penizek, V.; Pavlu, L.; Holubik, O.; Nemecek, K.; Houska, J.; Drabek, O.; Ash, C. Isotopic Tracing of Thallium Contamination in Soils Affected by Emissions from Coal-Fired Power Plants. Environ. Sci. Technol. 2016;50:9864-9871

Viers, J.; Grande Gil, J.A.; Zouiten, C.; Freydier, R.; Masbou, J.; Valente, T.; Torre, M.L.D.L.; Destrigneville, C.; Pokrovsky, O.S. Are Cu isotopes a useful tool to trace metal sources and processes in acid mine drainage (AMD) context? Chemosphere 2018;193:1071-1079

Viers, J.; Oliva, P.; Nonell, A.; Gélabert, A.; Sonke, J.E.; Freydier, R.; Gainville, R.; Dupré, B. Evidence of Zn isotopic fractionation in a soil-plant system of a pristine tropical watershed (Nsimi, Cameroon). Chem. Geol. 2007;239:124-137

Vogl, J.; Pritzkow, W. Isotope reference materials for present and future isotope research. J. Anal. At. Spectrom. 2010;25:923-932

Walder, A.J.; Platzner, I.; Freedman, P.A. Isotope ratio measurement of lead, neodymium and neodymium-samarium mixtures, hafnium and hafnium-lutetium mixtures with a double focusing multiple collector inductively coupled plasma mass spectrometer. J. Anal. At. Spectrom. 1993;8:19-23

Wall, A.J.; Mathur, R.; Post, J.E.; Heaney, P.J. Cu isotope fractionation during bornite dissolution: An in situ X-ray diffraction analysis. Ore Geol. Rev. 2011;42:62-70

Wang, D.; Zheng, Y.; Mathur, R.; Yu, M. Fractionation of cadmium isotope caused by vapour-liquid partitioning in hydrothermal ore-forming system: A case study of the Zhaxikang Sb–Pb–Zn–Ag deposit in Southern Tibet. Ore Geol. Rev. 2020a;119

Wang, J.; Su, J.; Li, Z.; Liu, B.; Cheng, G.; Jiang, Y.; Li, Y.; Zhou, S.; Yuan, W. Source apportionment of heavy metal and their health risks in soil-dustfall-plant system nearby a typical non-ferrous metal mining area of Tongling, Eastern China. Environ. Pollut. 2019a;254

Wang, L.; Li, X.; Tsang, D.C.W.; Jin, F.; Hou, D. Green remediation of Cd and Hg contaminated soil using humic acid modified montmorillonite: Immobilization performance under accelerated ageing conditions. J. Hazard. Mater. 2020b;387

Wang, L.; O'Connor, D.; Rinklebe, J.r.; Ok, Y.S.; Tsang, D.C.; Shen, Z.; Hou, D. Biochar Aging: Mechanisms, Physicochemical Changes, Assessment, And Implications for Field Applications. Environmental Science & Technology 2020c;

Wang, L.; Ok, Y.S.; Tsang, D.C.; Alessi, D.S.; Rinklebe, J.; Wang, H.; Mašek, O.; Hou, R.; O'Connor, D.; Hou, D. New Trends in Biochar Pyrolysis and Modification Strategies: Feedstock, Pyrolysis Conditions, Sustainability Concerns and Implications for Soil Amendment. Soil Use and Management 2020d;36:358-386

Wang, P.C.; Li, Z.G.; Liu, J.L.; Bi, X.Y.; Ning, Y.Q.; Yang, S.C.; Yang, X.J. Apportionment of sources of heavy metals to agricultural soils using isotope fingerprints and multivariate statistical analyses. Environ. Pollut. 2019b;249:208-216

Wang, S.; Hu, G.; Yan, Y.; Wang, S.; Yu, R.; Cui, J. Source apportionment of metal elements in PM2.5 in a coastal city in Southeast China: Combined Pb-Sr-Nd isotopes with PMF method. Atmos. Environ. 2019c;198:302-312

Wang, Y.N.; O'Connor, D.; Shen, Z.T.; Lo, I.M.C.; Tsang, D.C.W.; Pehkonen, S.; Pu, S.Y.; Hou, D.Y. Green synthesis of nanoparticles for the remediation of contaminated waters and soils: Constituents, synthesizing methods, and influencing factors. J. Clean Prod. 2019d;226:540-549

Wang, Z.; Coyte, R.M.; Dwyer, G.S.; Ruhl, L.S.; Hsu-Kim, H.; Hower, J.C.; Vengosh, A. Distinction of strontium isotope ratios between water-soluble and bulk coal fly ash from the United States. Int. J. Coal Geol. 2020e;222

Wei, R.; Guo, Q.; Yu, G.; Kong, J.; Li, S.; Song, Z.; Hu, J.; Tian, L.; Han, X.; Okoli, C.P. Stable isotope fractionation during uptake and translocation of cadmium by tolerant Ricinus communis and hyperaccumulator Solanum nigrum as influenced by EDTA. Environ. Pollut. 2018;236:634-644

Weiss, D.J.; Rausch, N.; Mason, T.F.D.; Coles, B.J.; Wilkinson, J.J.; Ukonmaanaho, L.; Arnold, T.; Nieminen, T.M. Atmospheric deposition and isotope biogeochemistry of zinc in ombrotrophic peat. Geochim. Cosmochim. Acta 2007;71:3498-3517

Weiss, D.J.; Rehkämper, M.; Schoenberg, R.; McLaughlin, M.; Kirby, J.; Campbell, P.G.C.; Arnold, T.; Chapman, J.; Peel, K.; Gioia, S. Application of nontraditional stable-isotope systems to the study of sources and fate of metals in the environment. Environ. Sci. Technol. 2008;42:655-664

Wen, H.; Zhang, Y.; Cloquet, C.; Zhu, C.; Fan, H.; Luo, C. Tracing sources of pollution in soils from the Jinding Pb-Zn mining district in China using cadmium and lead isotopes. Appl. Geochem. 2015;52:147-154

Wen, Y.; Li, W.; Yang, Z.; Zhang, Q.; Ji, J. Enrichment and source identification of Cd and other heavy metals in soils with high geochemical background in the karst region, Southwestern China. Chemosphere 2020;245

White, W.M. Isotope geochemistry. Chichester, West Sussex : John Wiley & Sons, Inc.; 2015

WHO. Ten chemicals of major health concern. World Health Organization 2017;

Widory, D.; Liu, X.; Dong, S. Isotopes as tracers of sources of lead and strontium in aerosols (TSP & PM2.5) in Beijing. Atmos. Environ. 2010;44:3679-3687

Wiederhold, J.G. Metal stable isotope signatures as tracers in environmental geochemistry. Environ. Sci. Technol. 2015;49:2606-2624

Wiederhold, J.G.; Smith, R.S.; Siebner, H.; Jew, A.D.; Brown, G.E.; Bourdon, B.; Kretzschmar, R. Mercury isotope signatures as tracers for Hg cycling at the new idria Hg mine. Environ. Sci. Technol. 2013;47:6137-6145

Wiggenhauser, M.; Bigalke, M.; Imseng, M.; Keller, A.; Rehkamper, M.; Wilcke, W.; Frossard, E. Using isotopes to trace freshly applied cadmium through mineral phosphorus fertilization in soil-

fertilizer-plant systems. Sci. Total Environ. 2019;648:779-786
Wilcke, W.; Krauss, M.; Kobza, J.; Zech, W. Quantification of anthropogenic lead in Slovak forest and arable soils along a deposition gradient with stable lead isotope ratios. J. Plant Nutr. Soil Sci. 2001;164:303-307
Wilson, M.; Wilson, D.L.; Mathur, R. Tracing the source of native copper mineral specimens with copper isotope values. Rocks Miner. 2016;91:352-356
Xia, Y.; Gao, T.; Liu, Y.; Wang, Z.; Liu, C.; Wu, Q.; Qi, M.; Lv, Y.; Li, F. Zinc isotope revealing zinc's sources and transport processes in karst region. Sci. Total Environ. 2020;724
Xiao, X.; Zhang, J.; Wang, H.; Han, X.; Ma, J.; Ma, Y.; Luan, H. Distribution and health risk assessment of potentially toxic elements in soils around coal industrial areas: A global meta-analysis. Sci. Total Environ. 2020;713
Xie, S.; Yang, F.; Feng, H.; Wei, C.; Wu, F. Assessment of Potential Heavy Metal Contamination in the Peri-urban Agricultural Soils of 31 Provincial Capital Cities in China. Environ. Manage. 2019;64:366-380
Xu, C.; Zhong, H.; Hu, R.Z.; Wen, H.J.; Zhu, W.G.; Bai, Z.J.; Fan, H.F.; Li, F.F.; Zhou, T. Sources and ore-forming fluid pathways of carbonate-hosted Pb–Zn deposits in Southwest China: implications of Pb–Zn–S–Cd isotopic compositions. Miner. Deposita 2020;55:491-513
Yang, L. Accurate and precise determination of isotopic ratios by mc-icp-ms: A review. Mass Spectrom. Rev. 2009;28:990-1011
Yang, L.; Tong, S.; Zhou, L.; Hu, Z.; Mester, Z.; Meija, J. A critical review on isotopic fractionation correction methods for accurate isotope amount ratio measurements by MC-ICP-MS. J. Anal. At. Spectrom. 2018;33:1849-1861
Yin, N.H.; van Hullebusch, E.D.; Benedetti, M.; Lens, P.N.L.; Sivry, Y. Zn isotopes fractionation during slags' weathering: One source of contamination, multiple isotopic signatures. Chemosphere 2018;195:483-490
Yin, R.; Deng, C.; Lehmann, B.; Sun, G.; Lepak, R.F.; Hurley, J.P.; Zhao, C.; Xu, G.; Tan, Q.; Xie, Z.; Hu, R. Magmatic-Hydrothermal Origin of Mercury in Carlin-style and Epithermal Gold Deposits in China: Evidence from Mercury Stable Isotopes. ACS Earth Space Chem. 2019;3:1631-1639
Yin, R.; Feng, X.; Li, X.; Yu, B.; Du, B. Trends and advances in mercury stable isotopes as a geochemical tracer. Trends Environ. Anal. Chem. 2014;2:1-10
Yin, R.; Feng, X.; Meng, B. Stable mercury isotope variation in rice plants (Oryza sativa L.) from the Wanshan mercury Mining District, SW China. Environ. Sci. Technol. 2013a;47:2238-2245
Yin, R.; Feng, X.; Wang, J.; Li, P.; Liu, J.; Zhang, Y.; Chen, J.; Zheng, L.; Hu, T. Mercury speciation and mercury isotope fractionation during ore roasting process and their implication to source identification of downstream sediment in the Wanshan mercury mining area, SW China. Chem. Geol. 2013b;336:72-79
Yin, R.; Pan, X.; Deng, C.; Sun, G.; Kwon, S.Y.; Lepak, R.F.; Hurley, J.P. Consistent trace element distribution and mercury isotopic signature between a shallow buried volcanic-hosted epithermal gold deposit and its weathered horizon. Environ. Pollut. 2020;259
Yuan, S.; Chen, J.; Cai, H.; Yuan, W.; Wang, Z.; Huang, Q.; Liu, Y.; Wu, X. Sequential samples reveal significant variation of mercury isotope ratios during single rainfall events. Sci. Total Environ. 2018;624:133-144

Zeng, J.; Han, G. Preliminary copper isotope study on particulate matter in Zhujiang River, southwest China: Application for source identification. Ecotoxicol. Environ. Saf. 2020;198

Zerkle, A.L.; Yin, R.; Chen, C.; Li, X.; Izon, G.J.; Grasby, S.E. Anomalous fractionation of mercury isotopes in the Late Archean atmosphere. Nat. Commun. 2020;11

Zhang, T.; Yang, Y.H.; Ni, J.P.; Xie, D.T. Best management practices for agricultural non-point source pollution in a small watershed based on the AnnAGNPS model. Soil Use Manage. 2019a:13

Zhang, Y.; Chen, J.; Zheng, W.; Sun, R.; Yuan, S.; Cai, H.; Yang, D.A.; Yuan, W.; Meng, M.; Wang, Z.; Liu, Y.; Liu, J. Mercury isotope compositions in large anthropogenically impacted Pearl River, South China. Ecotoxicol. Environ. Saf. 2020a;191

Zhang, Y.; Hou, D.; O'Connor, D.; Shen, Z.; Shi, P.; Ok, Y.S.; Tsang, D.C.W.; Wen, Y.; Luo, M. Lead contamination in Chinese surface soils: Source identification, spatial-temporal distribution and associated health risks. Crit. Rev. Environ. Sci. Technol. 2019b;49:1386-1423

Zhang, Y.; O'Connor, D.; Xu, W.; Hou, D. Blood lead levels among Chinese children: The shifting influence of industry, traffic, and e-waste over three decades. Environ. Int. 2020b;135

Zhao, L.; Hu, G.; Yan, Y.; Yu, R.; Cui, J.; Wang, X.; Yan, Y. Source apportionment of heavy metals in urban road dust in a continental city of eastern China: Using Pb and Sr isotopes combined with multivariate statistical analysis. Atmos. Environ. 2019a;201:201-211

Zhao, Y.; Xue, C.; Liu, S.A.; Mathur, R.; Zhao, X.; Yang, Y.; Dai, J.; Man, R.; Liu, X. Redox reactions control Cu and Fe isotope fractionation in a magmatic Ni–Cu mineralization system. Geochim. Cosmochim. Acta 2019b;249:42-58

Zhou, J.-W.; Li, Z.; Liu, M.-S.; Yu, H.-M.; Wu, L.-H.; Huang, F.; Luo, Y.-M.; Christie, P. Cadmium Isotopic Fractionation in the Soil–Plant System during Repeated Phytoextraction with a Cadmium Hyperaccumulating Plant Species. Environ. Sci. Technol. 2020;

Zhou, Y.; Sun, J.; Wang, L.; Zhu, G.; Li, M.; Liu, J.; Li, Z.; Gong, H.; Wu, C.; Yin, G. Multiple classes of chemical contaminants in soil from an e-waste disposal site in China: Occurrence and spatial distribution. Sci. Total Environ. 2021;752

Zhu, C.; Wen, H.; Zhang, Y.; Fan, H. Cadmium and sulfur isotopic compositions of the Tianbaoshan Zn-Pb-Cd deposit, Sichuan Province, China. Ore Geol. Rev. 2016;76:152-162

Zhu, C.; Wen, H.; Zhang, Y.; Fu, S.; Fan, H.; Cloquet, C. Cadmium isotope fractionation in the Fule Mississippi Valley-type deposit, Southwest China. Miner. Deposita 2017;52:675-686

Zhu, X.K.; O'Nions, R.K.; Guo, Y.; Belshaw, N.S.; Rickard, D. Determination of natural Cu-isotope variation by plasma-source mass spectrometry: Implications for use as geochemical tracers. Chem. Geol. 2000;163:139-149

Zieliński, M.; Dopieralska, J.; Belka, Z.; Walczak, A.; Siepak, M.; Jakubowicz, M. Sr isotope tracing of multiple water sources in a complex river system, Noteć River, central Poland. Sci. Total Environ. 2016;548-549:307-316